ARL 63-139

INVESTIGATION OF SURFACE ENERGY STATES OF SINGLE CRYSTAL METALS

R. [illegible]MENARD
A. [illegible]ANDERSON

GENERAL MILLS, INC. ELECTRONICS DIVISION
AEROSPACE RESEARCH
ST. PAUL, MINNESOTA

AUGUST 1963

AEROSPACE RESEARCH LABORATORIES
OFFICE OF AEROSPACE RESEARCH
UNITED STATES AIR FORCE

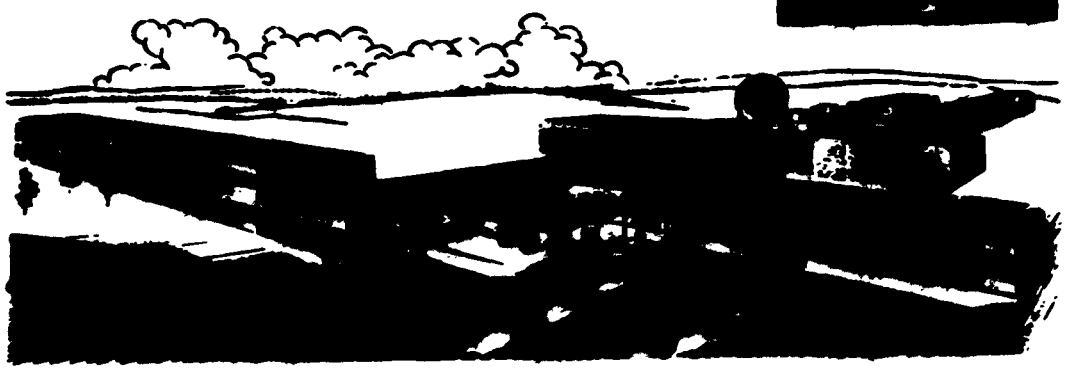

NOTICES

When Government drawings, specifications, or other data are used for any purpose other than in connection with a definitely related Government procurement operation, the United States Government thereby incurs no responsibility nor any obligation whatsoever; and the fact that the Government may have formulated, furnished, or in any way supplied the said drawings, specifications, or other data, is not to be regarded by implication or otherwise as in any manner licensing the holder or any other person or corporation, or conveying any rights or permission to manufacture, use, or sell any patented invention that may in any way be related thereto.

- - - - - - - - -

Qualified requesters may obtain copies of this report from the Defense Documentation Center, (DDC), Cameron Station, Alexandria, Virginia.

- - - - - - - - -

This report has been released to the Office of Technical Services, U. S. Department of Commerce, Washington 25, D. C. for sale to the general public.

- - - - - - - - -

Copies of ARL Technical Documentary Reports should not be returned to Aerospace Research Laboratories unless return is required by security considerations, contractural obligations or notices on a specified document.

300 - October 1963 - 8-142-162

ARL 63-139

INVESTIGATION OF SURFACE ENERGY STATES OF SINGLE CRYSTAL METALS

R. C. MENARD and A. A. ANDERSON

GENERAL MILLS, INC. ELECTRONICS DIVISION
AEROSPACE RESEARCH
ST. PAUL, MINNESOTA

AUGUST 1963

Contract AF 33(657)-8038
Project 7022
Task 7022-01

AEROSPACE RESEARCH LABORATORIES
OFFICE OF AEROSPACE RESEARCH
UNITED STATES AIR FORCE
WRIGHT-PATTERSON AIR FORCE BASE, OHIO

FOREWORD

This is an interim technical report of work performed by the Electronics Division of General Mills, Inc., Minneapolis, Minnesota, on Contract AF 33 (657)-8038 for the Aerospace Research Laboratories, Office of Aerospace, Research United States Air Force. The work was accomplished on Task 7022-01, "Research in Physical Properties of Surfaces and Films" of Project 7022, "Surface and Interface Phenomena of Matter" under the direction of Lt. E. L. Kern of the Chemistry Research Laboratory of ARL.

Work on the contract was performed between 15 January 1962 and 15 January 1963. This report contains the results of research conducted during Parts I and II of a three-part program, Part III of which is scheduled for completion on 15 November 1963. Part III will be the subject of a separate ARL technical report.

The authors wish to express their gratitude to Mr. W. Roepke and Mr. P. Preese, without whose technical assistance the work reported herein could not have been accomplished successfully.

ABSTRACT

A unique ion beam sputter cleaning apparatus has been developed to operate in a high vacuum system. This apparatus, known as a unoplasmatron, creates positive ions from various gases and focuses them into a beam of controlled density and energy. Bombarding ion currents of 80 microamps have been attained. Experiments have shown that this current is sufficient to produce large, smooth, brightly-etched surfaces on copper specimens in less than 1 hour.

A contact potential device has also been developed to study the surface energy of single-crystal metals in a vacuum. This device utilizes the vibrating condenser technique. Contact potential measurements of polycrystalline copper in this laboratory compare favorably with measurements reported in the literature. The changing contact potential of a clean titanium surface exposed to air has been measured. The contact potential varied from about 230 mv to 330 mv. The accuracy of these measurements is believed to be about ±5 mv.

TABLE OF CONTENTS

LIST OF ILLUSTRATIONS

LIST OF ILLUSTRATIONS (continued)

LIST OF TABLES

INTRODUCTION

This is a summary technical report of Parts I and II of a three-part research program being accomplished under Contract AF 33(657)-8038, and presents the results of investigations carried out during the period 15 January 1962 to 15 January 1963.* The objectives of this program have been

1) To construct a compact, very-high-vacuum system with an associated ion bombardment facility and a sensitive friction probe,

2) To prepare selected single-crystal surfaces by standard X-ray and polishing techniques,

3) To clean the single-crystal surfaces with argon ion bombardment in a high vacuum,

4) To determine the friction coefficient and surface potentials of the clean single crystals as a function of lattice structure and crystal orientation using the sensitive friction probe and a contact potential device,

5) To examine the surfaces with an optical microscope (or where feasible the electron mirror microscope) to determine contact area and nature of surface damage subsequent to friction measurements, and

6) To analyze the characteristics of friction and surface deformation in terms of surface energy of the contacting materials, and to correlate the results with lattice structure and crystallographic orientation.

Work accomplished during this period included design, construction, and evaluation of a very-high-vacuum system, an ion bombardment facility, a sensitive friction probe, and a contact potential measuring device. Preliminary experiments with these apparatus were accomplished, and are described herein.

PART I

SYSTEM DESIGN AND SAMPLE PREPARATION

DESIGN OF A VERY-HIGH-VACUUM SYSTEM

Probably the most serious difficulties faced by workers in the field of surface research are the rapid recontamination of fresh surfaces and the difficulty of producing initially clean surfaces with reproducible properties. Background pressures of 10^{-8} Torr or better must be attained where contamination-free surfaces are required. With proper trap designs and pumps of large enough capacities, it is possible to design oil-pumped systems that will perform adequately in this pressure region. Figure 1 is a schematic diagram of the very-high-vacuum system that was built for this program to combat the contamination problem. In

*Manuscript released 15 May 1963 by the authors for publication as an ARL Technical Documentary Report.

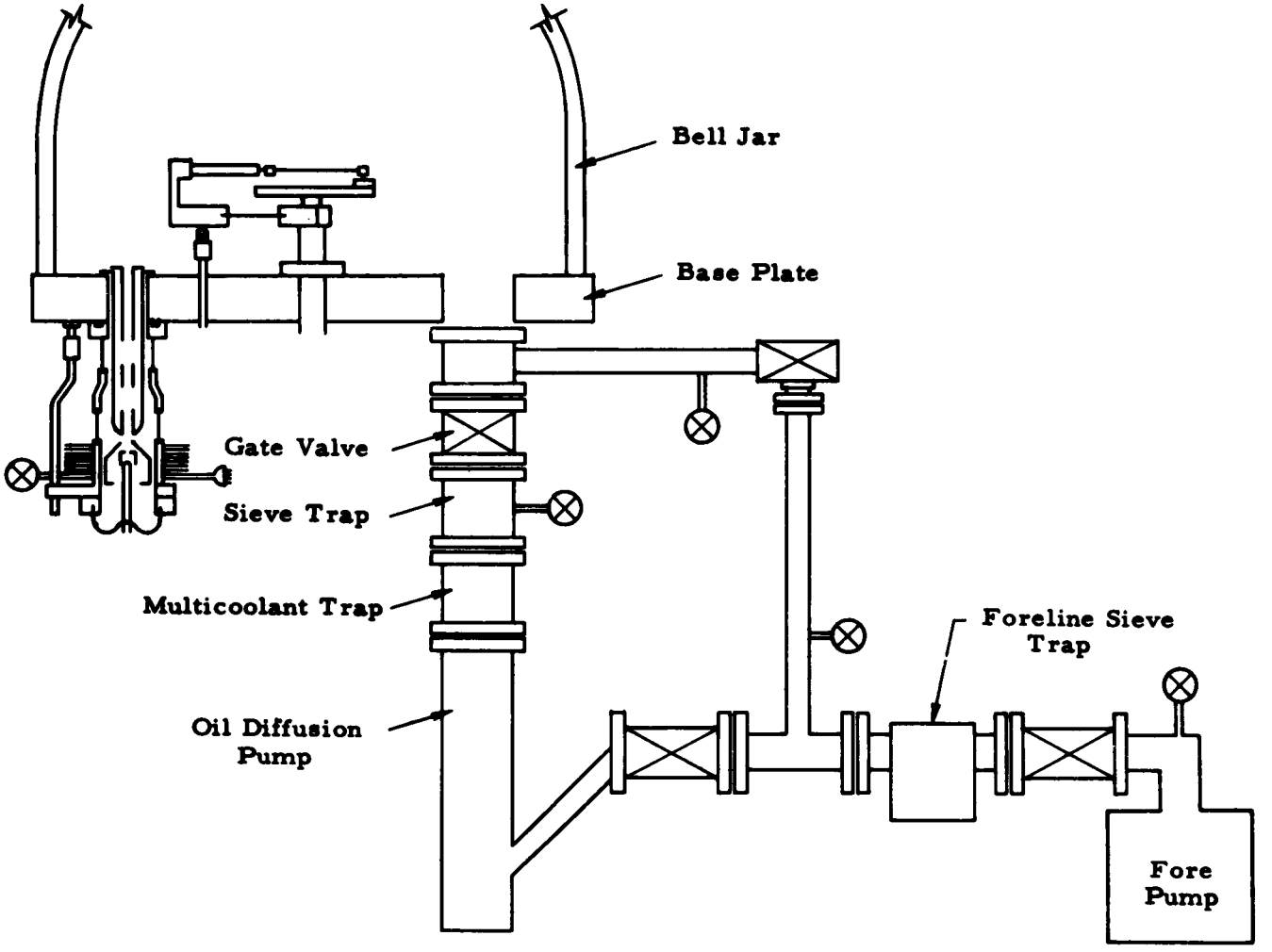

Figure 1. Very High Vacuum System

designing the pumping system, maximum use was made of advanced state-of-the art components. The high side of the pumping system includes a 2-inch water-cooled, oil diffusion pump (rated speed 115 liters per sec), a 2-inch multicoolant baffle trap, a 2-inch sieve trap, and a 2-inch gate valve in the main line, all made by Consolidated Vacuum Corporation. A unique feature of this system is the dual trapping to isolate the diffusion pump. Stainless steel plumbing, 6-bolt flanges, and Viton O-ring seals are used throughout the high side. The diffusion pump is backed up by a Welch 5 cfm forepump isolated with a 1-inch Ultek foreline sieve trap.

The enclosure consists of a pyrex glass bell jar and a stainless steel base plate. The bell jar (made by Dow Corning) is 12 inches in diameter and 12 inches in height. The base plate is 15 inches in diameter by 7/8-inch thick, custom made from No. 304 stainless steel, and polished to 20 microinches on both sides.

In addition to a 2-inch main pump port, ten smaller ports are provided. There are four high-voltage feedthroughs and two clusters of ten low-voltage feedthroughs for instrumentation. Rotary motion is available through an Ultek magnetically-coupled feedthrough, and precise vertical motion is obtained with a bellows-sealed micrometer feedthrough. The gauge port has a manifold with provisions for a thermocouple and an ion gauge. The remaining port is used by the unoplasmatron ion source. To date we have attained background pressures of 2×10^{-7} Torr in this system without use of a cold trap.

SOLID SURFACE CLEANING

Definition of a Clean Surface

After the background pressure around the specimen surfaces has been reduced to a very low level, it is still necessary to clean the surfaces. From the standpoint of cleanliness, solid surfaces can be divided into three groups--namely, pure surfaces, clean surfaces, and technical surfaces. These surfaces have the following characteristics:

1) Pure Surfaces - Sometimes called "atomically clean", these surfaces are characterized by the complete absence of adsorbed films, either inorganic or organic. Such surfaces can be created in an ultrahigh vacuum (10^{-9} Torr or higher), by cleavage, or by a combination of high temperature outgassing and ion bombardment.

2) Clean Surfaces - These surfaces are free of water vapor and organic contamination but may have physically and chemically adsorbed gas films, particularly oxide films. Such surfaces can be created in a very high vacuum (10^{-6} to 10^{-9} Torr), by high temperature outgassing, or by ion bombardment.

3) Technical Surfaces - These surfaces are coated with adsorbed water vapor, hydrocarbons, or other reactive compounds. All surfaces exposed to the atmosphere are considered to be technical surfaces. Special technical surfaces can be created in a vacuum by exposing pure or clean surfaces to a reactive environment.

It is possible to prepare clean metal surfaces in a high vacuum with thermal methods alone. For example, Bowden and Tabor[1] have shown that the coefficient of friction of nickel surfaces rises as high as $\mu = 9$ after the surfaces have been heated in a vacuum to 1000 C. But the nature of such experiments is severely limited because the vacuum system and sample mountings must be able to withstand high temperatures.

In contrast, ion bombardment can be used to clean surfaces without resorting to such high temperatures. More versatile experiments can therefore be performed. In fact, Schlier and Farnsworth[2] have shown that an atomically clean surface can be produced and maintained under ultrahigh vacuum conditions with ion bombardment.

Ion Bombardment Cleaning

When atomic particles such as ions moving at high speed strike a solid surface, they cause the surface to disintegrate. This process is known as sputtering. The ratio of the number of atoms removed from the surface to the number of ions incident on the surface is the sputtering yield. Sputtering experiments are usually conducted in a gas-discharge apparatus of which there are three fundamental types: 1) glow discharge, 2) low pressure supported plasma, and 3) ion beam. The parameters which influence yield belong either to the gas discharge or to the solid-state aspect of the problem.[3] In the first group belong gas pressure, the nature of the ions, ion energy, ion current density, and angle of incidence of the bombarding ions. In the second group belong the nature of the target material, target temperature, target surface configuration, and orientation of exposed crystal faces.

Most sputtering yield data are presented in the form shown in Figure 2. The threshold energy is the intercept of the yield curve with the energy axis. In sputter cleaning, the object is to remove adsorbed material from the sample surface while preventing surface erosion that might adversely affect subsequent experiments.

All early experimental ion bombardment studies were performed in glow discharges of inert gases. In these experiments large bombarding current densities are possible. In addition, the ion bombardment rate can usually be made large compared with the bombardment rate of residual gases, so that target surfaces can be considered relatively clean. But if operating pressures rise above 0.1 Torr, back-scatter of sputtered material to the target can be significant. Bombarding energy is also difficult to control and measure in a glow discharge.

The limitations of glow discharge sputtering have been largely eliminated by the use of low pressure supported plasma techniques. A comprehensive review of these techniques has been given by Wehner.[3] Using thermionic or pool-type cathodes to support the plasma, sputtering can be accomplished at pressures of about 10^{-3} Torr. Back-scattering of sputtered material is eliminated at these pressures, and high-density, controlled energy ion currents are easily attained.

Recent experimental work has shown a trend toward ion-beam techniques. In these experiments, the beam energy, composition, and angle of incidence can be easily controlled, and high vacuums (10^{-5} Torr) have been maintained. In recent years several workers[5-7] have used ion beam techniques to prepare atomically clean surfaces in ultrahigh vacua. These surfaces remain atomically clean

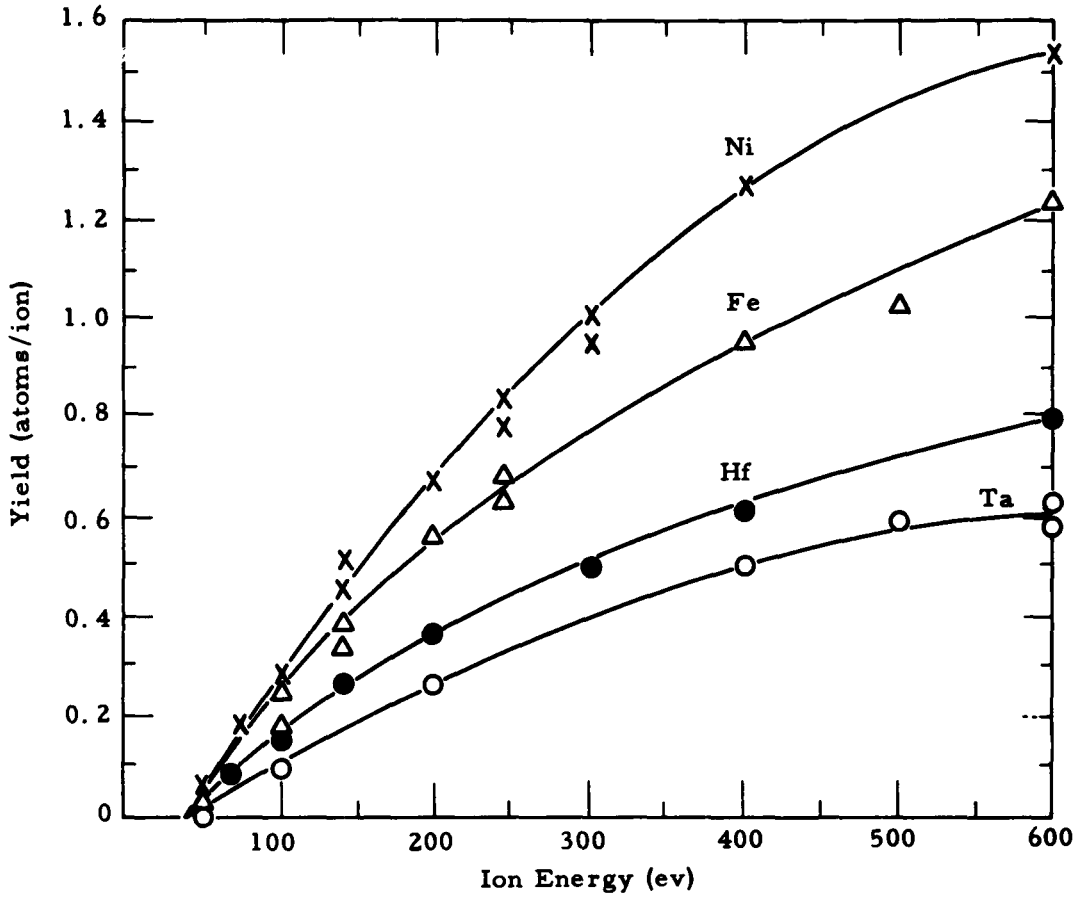

Figure 2. Representative Sputtering Yield Curves Obtained for Ni, Fe, Hf, and Ta in Argon (after Laegried and Wehner[4])

for some time since surface layers have no opportunity to rebuild. In the more common high vacuum systems, however, a steady-state balance is reached between destructive properties of the bombarding beam and regeneration of surface layers from residual gas in the system. Surfaces prepared in a high vacuum will remain quite clean if there is a low background of residual water vapor and hydrocarbons, i. e., if the system was initially evacuated to 10^{-8} to 10^{-9} Torr.

PREPARATION OF THE UNOPLASMATRON ION BOMBARDMENT APPARATUS

The unoplasmatron ion source is an electronic device which creates positive ions from various gases and focuses them into a beam of controlled density and energy. As an auxiliary unit in a vacuum system, it can be used to bombard specimen surfaces with high speed atomic particles that will remove adsorbed gases and vapors.

Theory of Operation

The unoplasmatron ion beam apparatus consists of two basic systems: 1) the ion generating system or source, and 2) the optical system or lenses.

The ion generating system itself is more properly known as the unoplasmatron.[8] The basic components of this system shown in Figure 3 are the cathode (A), the baffle (B), the anode (C), and the extractor (D). There are two limitations to the ion output of the unoplasmatron: 1) source limitation as affected by power input to the cathode, and 2) space charge limitation as predicted by the Langmuir-Child Law.[9,10]

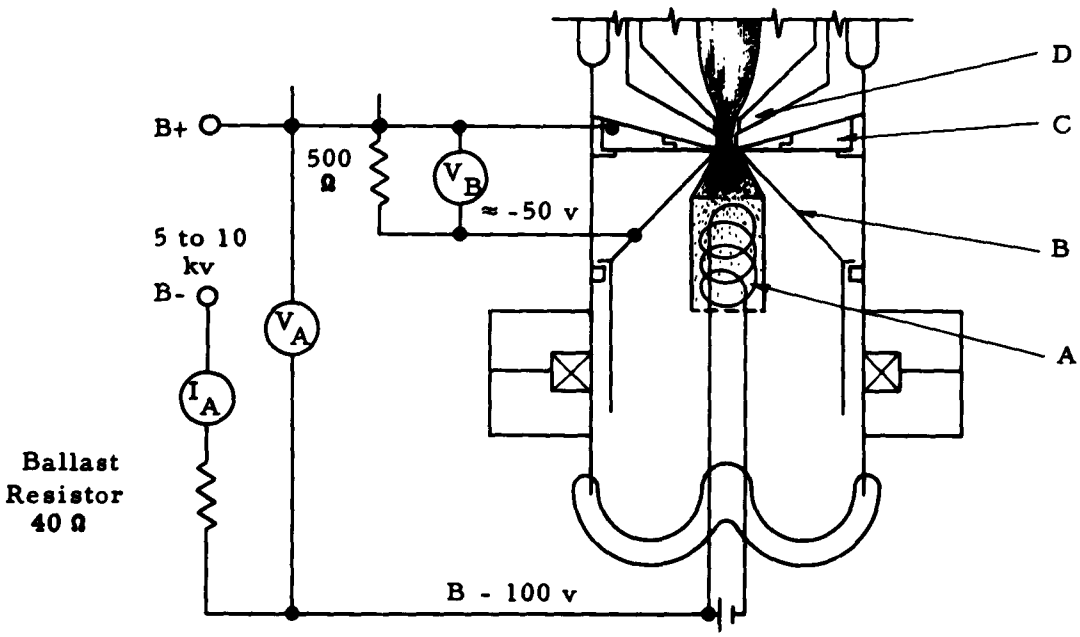

Figure 3. Unoplasmatron Ion Source

The electron current between the cathode and anode may be limited either by temperature of the cathode or by voltage between the electrodes as illustrated in Figure 4.

These plots show the variation in electron current observed from a tungsten filament 0.25 mm in diameter located along the axis of a cylinder 2.54 cm in diameter and 7.62 cm long. The maximum available electron current as a function of temperature is given by the Dushman equation[11]

$$J = A_o T^2 \epsilon_o - \frac{b_o}{T} \text{ amp/m}^2 \tag{1}$$

where J = current density in amperes/m^2 of cathode area

T = temperature of cathode in K

$$A_o = \frac{4\pi mek^2}{h^3} = \text{a constant}$$

$$b_o = \frac{eE_w}{k} = 11,600\ E_w = \text{a constant}$$

E_w = work function of cathode metal.

The factor A_o in theory should be a universal constant for all metals, having a value of 120.4×10^4 amp/m^2/deg^2. The values of A_o determined experimentally actually vary over a wide range. The reason for this variation is not known, although it may be because the metal surface does not approximate an infinite plane. Many metals (including tungsten) have a value of $A_o = 60.2 \times 10^4$ amp/m^2/deg^2.

The absolute temperature of a 1 mm diameter cathode as a function of cathode current is shown in Figure 5. Values of electron emission versus tungsten cathode temperature, as calculated from Eq (1), are shown in Table I. From Figure 5 and Table I it is possible to estimate the maximum ionization current available in the unoplasmatron for a given cathode current input.

Ideally, the maximum number of ions produced in such a source would be limited by space charge alone in a manner analogous to the limitation of current flow by the space charge. The essence of this derivation is given on page 10.

Consider a closed surface S enclosing a volume V within which are certain charges q_1, q_2 .... Form a surface integral as follows: Take an element da of the surface area. If $\bar{n}$ is a unit vector along the outer normal to the surface and $\bar{E}$ is the value of the electric intensity at da, then the surface integral is $\bar{E} \cdot \bar{n}$ da integrated over the surface S. From Gauss's theorem[13] it can be shown that

$$\bar{E} \cdot \bar{n}\ da = \sum_i \frac{q_i}{\epsilon_o} \tag{2}$$

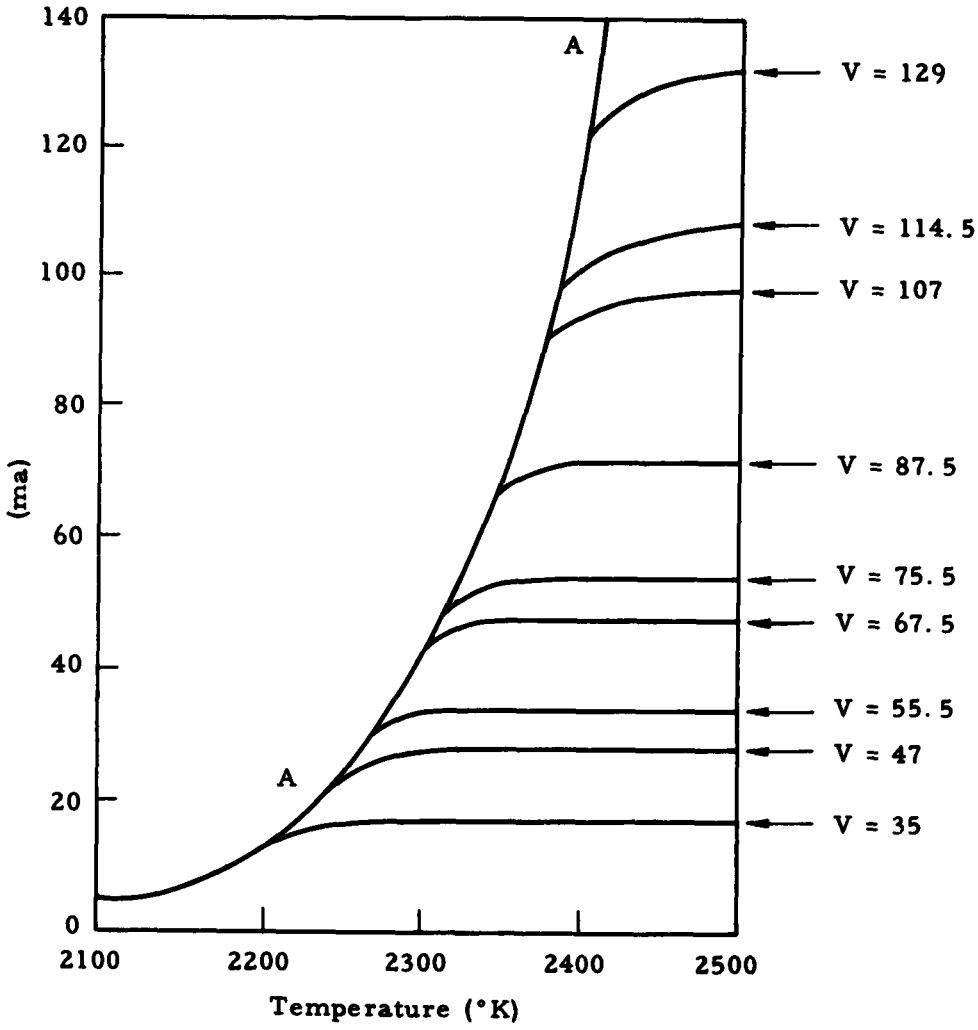

Figure 4. Limitation of Electron Current in a Hot-Cathode Diode by (a) Temperature of the Cathode, as Shown by the Curve AA, or (b) Anode Volts, as Shown by the Horizontal Lines for Different Values of the Anode Potential (after Dushman[11])

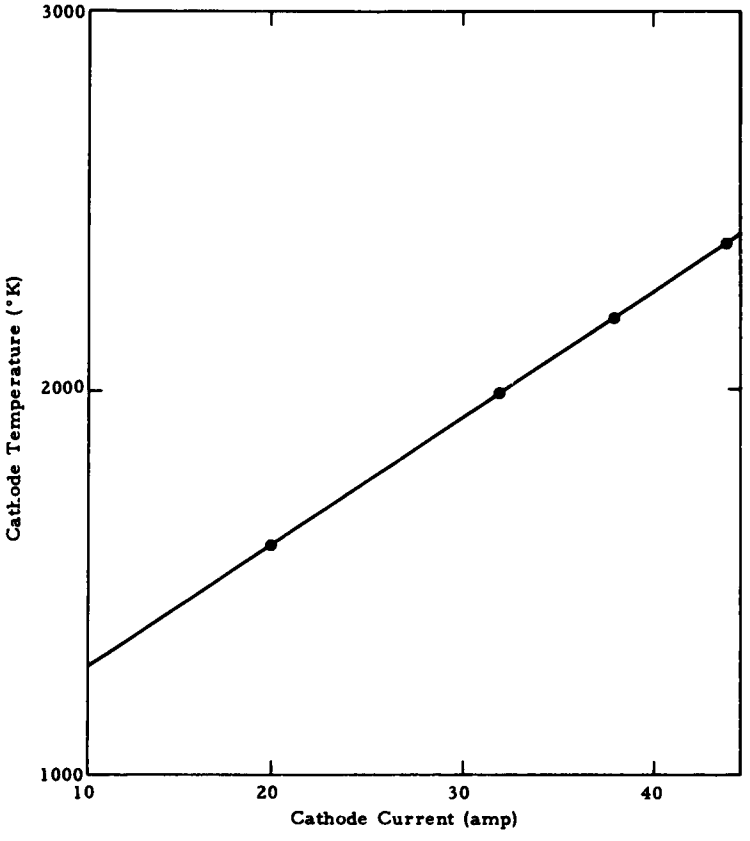

Figure 5. Relation between Current and Temperature for a 1 mm Diameter Incandescent Tungsten Wire in High Vacuum (after von Ardenne[12])

Table I. Electron Emission of a Tungsten Cathode

T (K)	I (amp/cm^2)	W (watts/cm^2)
1600	9.27×10^{-7}	7.74
1800	4.47×10^{-5}	14.2
2000	1.00×10^{-3}	24.0
2200	1.33×10^{-2}	38.2
2400	0.116	57.7
2600	0.716	83.8
2800	3.54	17.6
3000	14.15	160.5

After Dushman[11]

where $\epsilon_o = 8.85 \times 10^{-12}$ coulomb^2/newton-m^2 (permittivity of a vacuum).

If within the volume V there is a continuous distribution of volume charge rather than a discrete set of point charges, Eq (2) becomes

$$\int_S \bar{E} \cdot \bar{n}\, da = \frac{1}{\epsilon_o} \int_V \rho\, dv \tag{3}$$

where the volume integral is over the volume V enclosed by the surface S, and ρ is the charge per unit volume in coulombs per cm^3.

From the divergence theorem, we determine that

$$\int_S \bar{E} \cdot \bar{n}\, da = \int_V \text{div } E\, dv. \tag{4}$$

Combining (3) and (4), we obtain

$$\frac{1}{\epsilon_o} \int_V \rho\, dv = \int_V \text{div } \bar{E}\, dv, \tag{5}$$

which holds for any arbitrary volume V. This cannot be the case unless the integrands are equal, i.e., unless

$$\text{div } \bar{E} = \frac{\rho}{\epsilon_o}. \tag{6}$$

By definition

$$\bar{E} = - \text{grad } V \tag{7}$$

where V is the potential.

From Eqs (6) and (7), then, we have

$$\nabla^2 V = - \frac{\rho}{\epsilon_o}. \tag{8}$$

This is known as Poisson's equation in three dimensions.

Eq (8) written out is

$$\frac{\partial^2 V}{\partial x^2} + \frac{\partial^2 V}{\partial y^2} + \frac{\partial^2 V}{\partial x^2} = \frac{-\rho}{\epsilon_o} . \tag{9}$$

If it is now assumed that we have an electronic device in which the electric field is parallel in the x-direction, $\frac{\partial^2 V}{\partial y^2}$ and $\frac{\partial^2 V}{\partial z^2}$ are equal to zero. Then Eq (9) becomes

$$\frac{\partial^2 V}{\partial x^2} = - \frac{\rho}{\epsilon_o} . \tag{10}$$

This relation is known as Poisson's equation in one dimension.

Now assume a diode in which there are two infinitely large parallel plates positioned as shown in Figure 6.

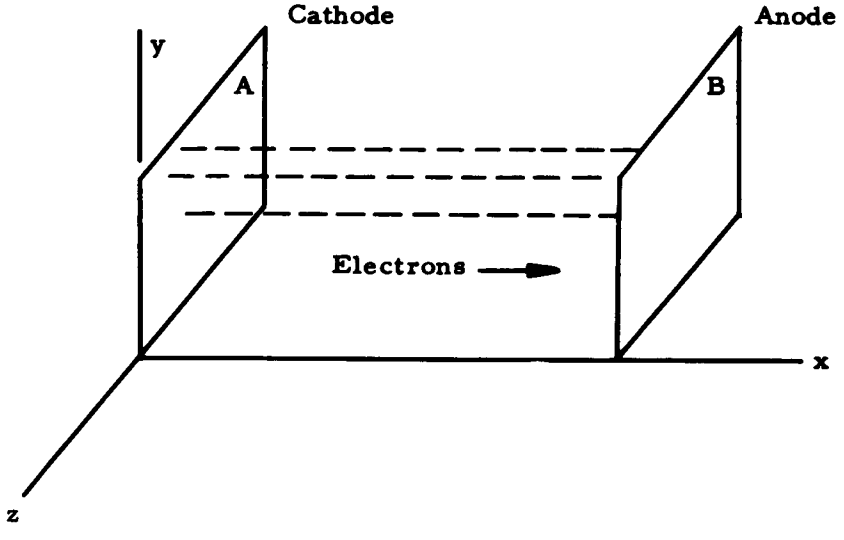

Figure 6. Parallel-Plate Diode

Let the left-hand plate at the origin be heated to a very high temperature so that emission will always be larger than the demand for electrons, or the current will never be temperature saturated. The right-hand plate, or anode, is left cold, and a positive potential V_b is applied to it with respect to the cathode. These two plates exist in a vacuum so that collisions of electrons with gas atoms need not be considered. Since the surfaces are infinite, edge effects of the electric field may be neglected, and the field will be uniform and everywhere perpendicular to the surfaces. Electrons emitted from A travel from A to B, attracted by the positive potential on B. If ρ is the density of charge per unit volume in the space between A and B and v is the average velocity of the charge, then the expression for current is

$$j = -\rho v . \tag{11}$$

The kinetic energy of an electron falling through an electric field is dependent on its energy of emission and the potential through which it has fallen, and can be determined from

$$\frac{mv^2}{2} = Ve + \frac{mv_o^2}{2} \tag{12}$$

where m = mass of the electron

v = velocity of the electron

V = the potential

e = charge of the electron

v_o = initial velocity of the electron.

The electron's initial energy $\frac{mv_o^2}{2}$ is usually about 1 ev, which is small compared to the energy acquired when it falls through potentials usually encountered in electronic devices. This energy may be neglected with respect to Ve. Using Eqs (11) and (12), we now modify Eq (10) to

$$\frac{d^2V}{dx^2} = \frac{j}{\epsilon_o v} = \frac{j}{\epsilon_o \sqrt{\frac{2Ve}{m}}} . \tag{13}$$

Multiplying both sides by $2\frac{dV}{dx}$, we get

$$\frac{2dV}{dx}\,\frac{d^2V}{dx^2} = \frac{2j}{\epsilon_o\sqrt{\frac{2e}{m}}}\,V^{-1/2}\,\frac{dV}{dx}. \tag{14}$$

Integration yields

$$\left(\frac{dV}{dx}\right)^2 = \frac{4j}{\epsilon_o\sqrt{\frac{2e}{m}}}\,V^{1/2} + C_1. \tag{15}$$

At the cathode's surface, where the potential V is zero, there is a small negative, or repelling field. The constant C_1 is therefore equal to the square of this small negative field. Experiments have shown that, although this field is actually present, it is so small that no appreciable error is introduced by neglecting the surface field as the constant C_1. The space charge is actually zero at some point very close to the cathode. For purposes of this analysis, then, the cathode surface is in effect moved out of this small distance.

Taking the square root of Eq (15) and rearranging terms, we have

$$V^{-1/4}\,dV = \frac{2}{\sqrt[4]{\frac{2e}{m}}}\,\sqrt{\frac{j}{\epsilon_o}}\,dx. \tag{16}$$

Integration now yields

$$4/3\,V^{3/4} = \frac{2}{\sqrt[4]{\frac{2e}{m}}}\,\sqrt{\frac{j}{\epsilon_o}}\,x + C_2 \tag{17}$$

in which if $x = 0$ and $V = 0$, $C_2 = 0$.

Selecting as particular values of potential and distance those at the anode V_b and d, Eq (17) may be written in terms of current density reaching the anode and becomes

$$j = \frac{\epsilon_o}{2.25}\,\sqrt{\frac{2e}{m}}\,\frac{V_b^{3/2}}{d^2}. \tag{18}$$

Eq (18) is known as the Langmuir-Child law, the three-halves power law, or the space-charge equation and applies for very large parallel-plane electrodes.

The Langmuir-Child law is used to predict the maximum ion flow that can be expected in the unoplasmatron. When Eq (18) is used to predict ion flow, the atomic weight M of the ionized gas is usually substituted for the elementary particle mass m. The atomic weight of an element is related to the elementary particle mass by the relationship

$$M = N_o m, \tag{19}$$

where N_o = Avogadro's number.

Combining Eqs (18) and (19) we have

$$j = \frac{\epsilon_o}{2.25} \sqrt{\frac{2eN_o}{M}} \frac{V_b^{3/2}}{d^2}, \tag{20}$$

and by putting in the values of the constants we obtain

$$j = 5.46 \times 10^{-5} \frac{V_b^{3/2}}{\sqrt{Md^2}} \text{ (ma/cm}^2\text{)} \tag{21}$$

where V_b = extraction potential in volts
M = atomic weight of the ions
d = distance between the anode and the extractor in cm

A log-log plot of maximum ion current j versus extractor voltage V_b as predicted by the Langmuir-Child law for argon is shown in Figure 7. One can see from Figure 7 that the extractor-anode separation has a pronounced effect on the total theoretical ion current. The actual output of the unoplasmatron source is limited by the cross-sectional area of the anode orifice (Figure 3C). In our device this orifice is about 0.1 cm in diameter. Thus, if j were 100 ma/cm^2, the actual source output would be approximately 0.79 ma.

When the ion beam leaves the extractor orifice, it begins to diverge because of the aperture effect. According to Zworykin,[14] an electron passing parallel to the axis through a cylindrical lens will emerge from the cylinder at an angle relative to the axis defined by

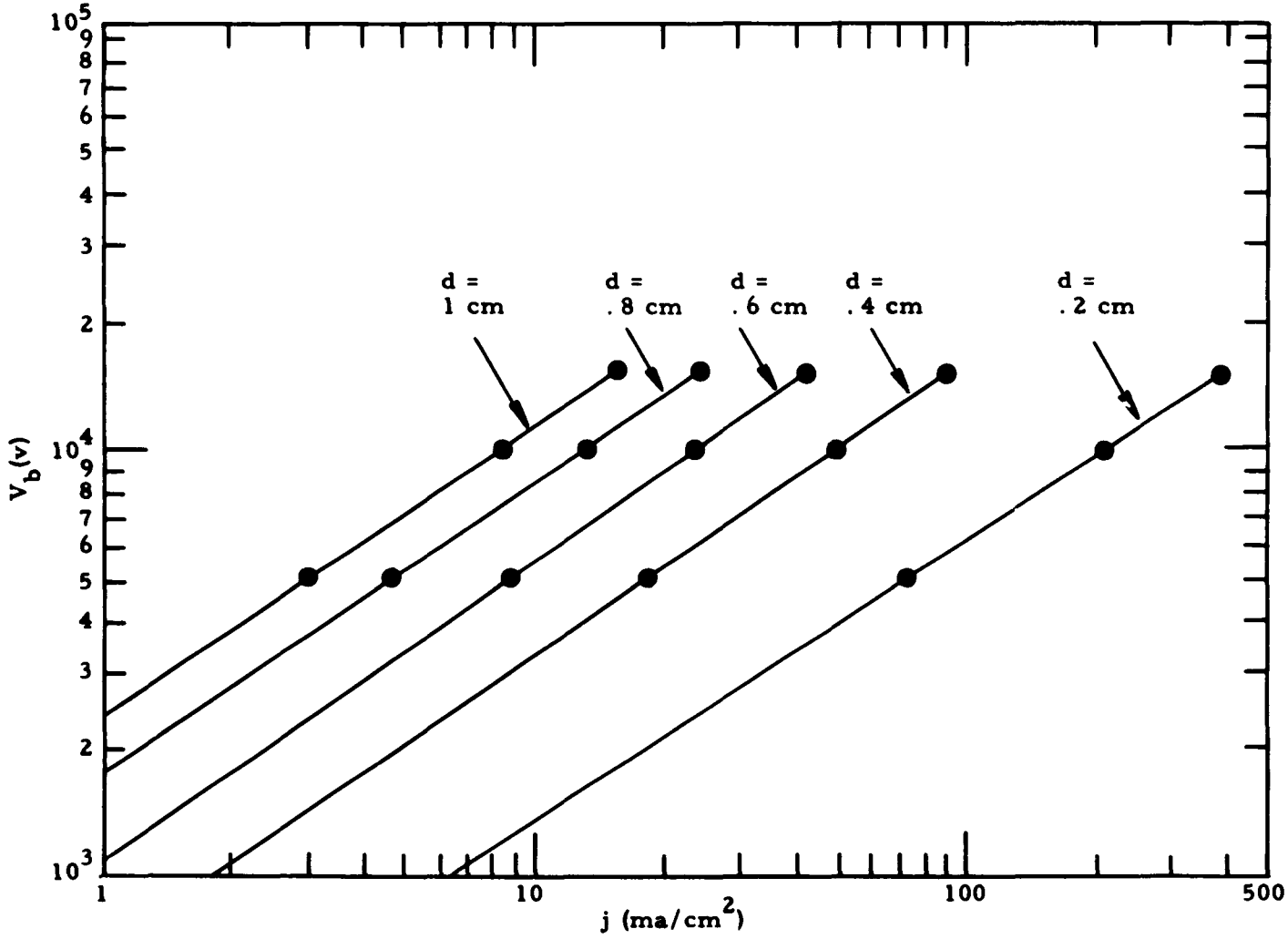

Figure 7. Plot of Maximum Ion Current (j) versus Extractor Voltage (V_b) as Predicted by the Langmuir-Child Law for Argon

$$\tan \alpha = -\frac{r}{f} \qquad (22)$$

where r = separation of the electron from the axis of the lens

f = focal length of the lens.

This condition is shown graphically in Figure 8 where the extractor opening can be considered a cylindrical, single-aperture lens. The optical system of the ion beam apparatus must first converge the ion beam after it leaves the extractor and then focus a parallel beam on the specimen.

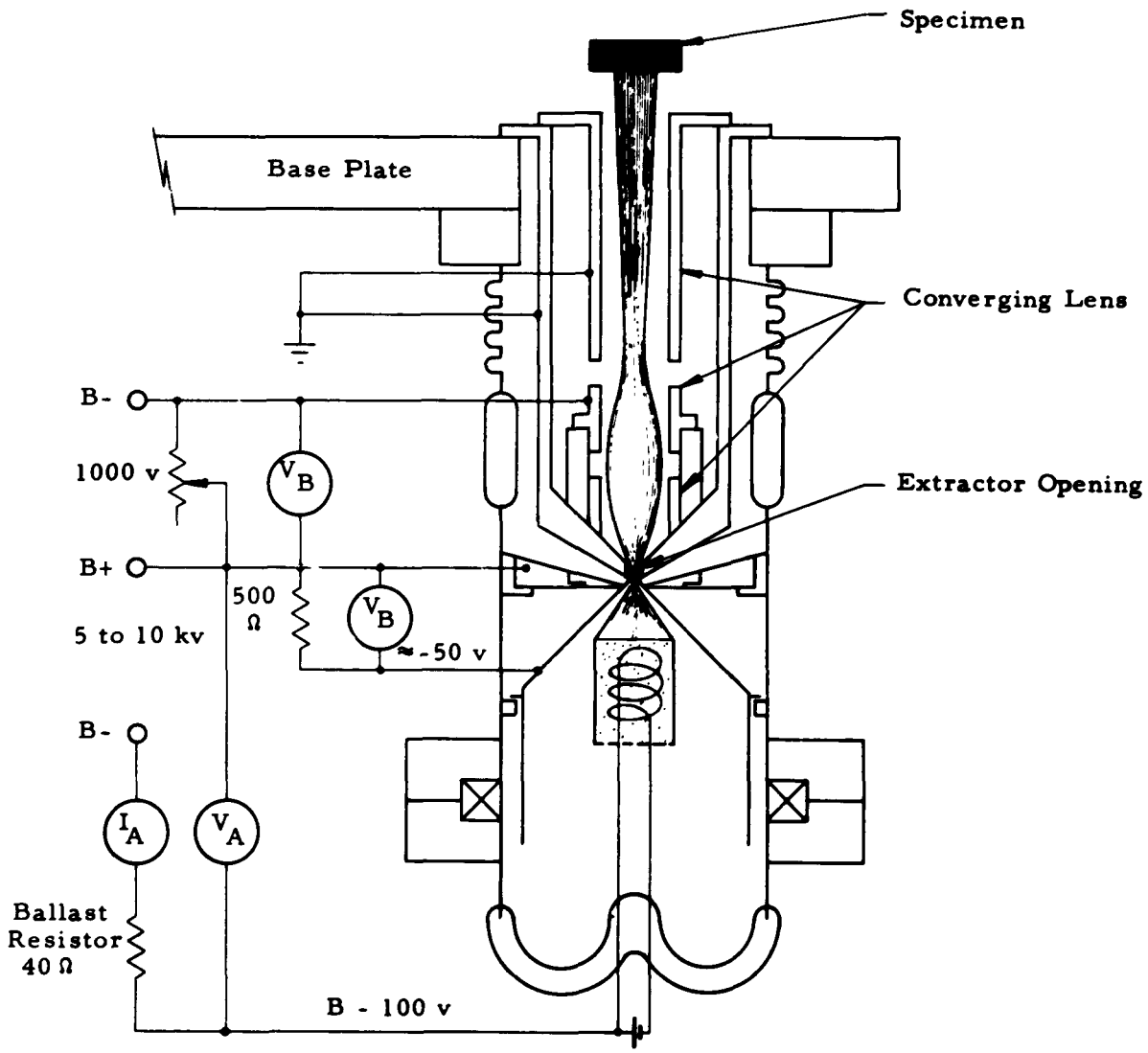

Figure 8. Unoplasmatron Ion Source and Optical System

The converging lens is a three-aperture lens known as a unipotential lens. The basic components of the unipotential lens are illustrated in Figure 9. As shown in this figure, a three-aperture lens consisting of a short cylinder between two cylinders at a different potential forms a converging lens whether the short cylinder is lower or higher in potential than the outer cylinders. The electron path shown by the solid lines in Figure 9 can be calculated by integration of the paraxial ray equation:

$$r'' = -\frac{\phi'}{2\phi} r' - \frac{\phi''}{4\phi} r \qquad (23)$$

where ϕ = potential along the axis ($r = 0$)

r = distance from the axis.

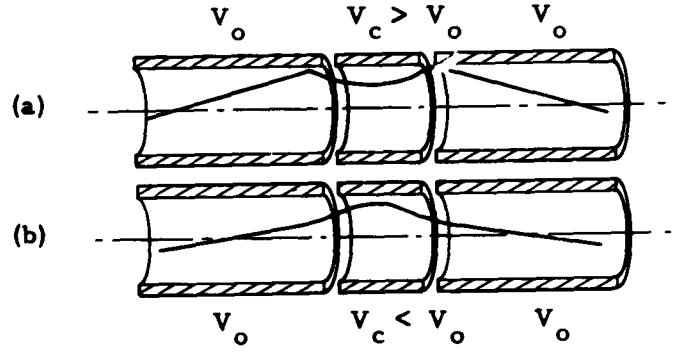

Figure 9. Lens Formation by a Short Cylinder between Two Cylinders at a Different Potential (after Pierce[15])
(Note that effect is converging regardless of potential gradient between cylinders.)

Figure 10 presents properties of a unipotential lens of the type described in Figure 9. The characteristic quantities plotted are the refractive power or reciprocal focal length 1/f, and the working distance or separation of the focal point from the plane of the nearest outer aperture. An examination of the refractive power curves indicates that for a given electron velocity a strong lens can be obtained more easily by making the central electrode negative with respect to the outer electrodes than by making it positive. Unipotential lenses therefore are normally operated with the central electrode at a potential which is low compared to that of the outer electrodes, as shown in Figure 9(a). The lowest potential of the central electrode for which such fields will act as lenses is that at which the axial potential at the center of the lens is just reduced to zero. For the lens described in Figure 10, this occurs at $V_c = 0.278\ V_o$. A practical limit is usually reached much earlier. The working distance should be positive and preferably about equal to the diameter of the outer aperture.[14] Proper adjustment of the ratio V_c/V_o will thus converge the ion beam after it leaves the extractor, as illustrated in Figure 8.

Experimental Design

The unoplasmatron ion source (Figure 11) is a low pressure type after M. von Ardenne.[16] It has high power efficiency, high ionization efficiency, and may be used with a variety of gases. It is composed of a demountable tungsten thermionic cathode (A), a tantalum heat shield (B), a tantalum constricting baffle (C), and a stainless steel anode (D) with molybdenum insert (E). These components are enclosed in a stainless steel cylinder (F). The glass-to-Kovar cathode feedthrough (G) is attached to the steel cylinder with stainless steel flanges and a copper shear-seal gasket (H).

To make an ion source of an arc-discharge device, some mechanism must be provided to extract ions from the discharge. The extraction system used here is a Pierce Gun[17] (I) and a single-potential lens (J). These two are situated in the container directly above the unoplasmatron ion source. A glass-to-Kovar seal (K) insulates the upper container that surrounds the extractor from the lower container that surrounds the arc-discharge. The exterior of the unoplasmatron is shown in Figure 12. The chief features shown there are the Kovar filament feedthrough (A), the high temperature insulating bakelite support (B), the gas inlet (C) with vernier needle valve adjustment (D), air cooling fins (E), insulating glass joint (F), and bellows expansion joint (G).

The electrical circuit diagram and the shape of the ion beam of the unoplasmatron ion source are also shown in Figure 11. In operation, a low-pressure arc-discharge is produced between the thermionic cathode (A) and the anode (D). The discharge is constricted by a baffle placed between the main electrodes. The effect of the baffle is to produce a greater ionization density than would be obtained in a free arc of like current.

A considerable voltage drop, about equal to the first ionization potential of the working gas, occurs within a short distance of the cathode. This region, the cathode fall region, is characterized by a strong positive space charge. At the other end of the discharge is the anode drop region characterized by a strong negative space charge. Between these two regions lies a positive column, a zone of small potential gradient and neutral charge. This column is a plasma. Nearly all ionization in the low-pressure arc occurs in the positive column. Primary electrons from the cathode are accelerated by the cathode fall, thus gaining enough energy to ionize neutral gas in the system The dense plasma produced is expelled

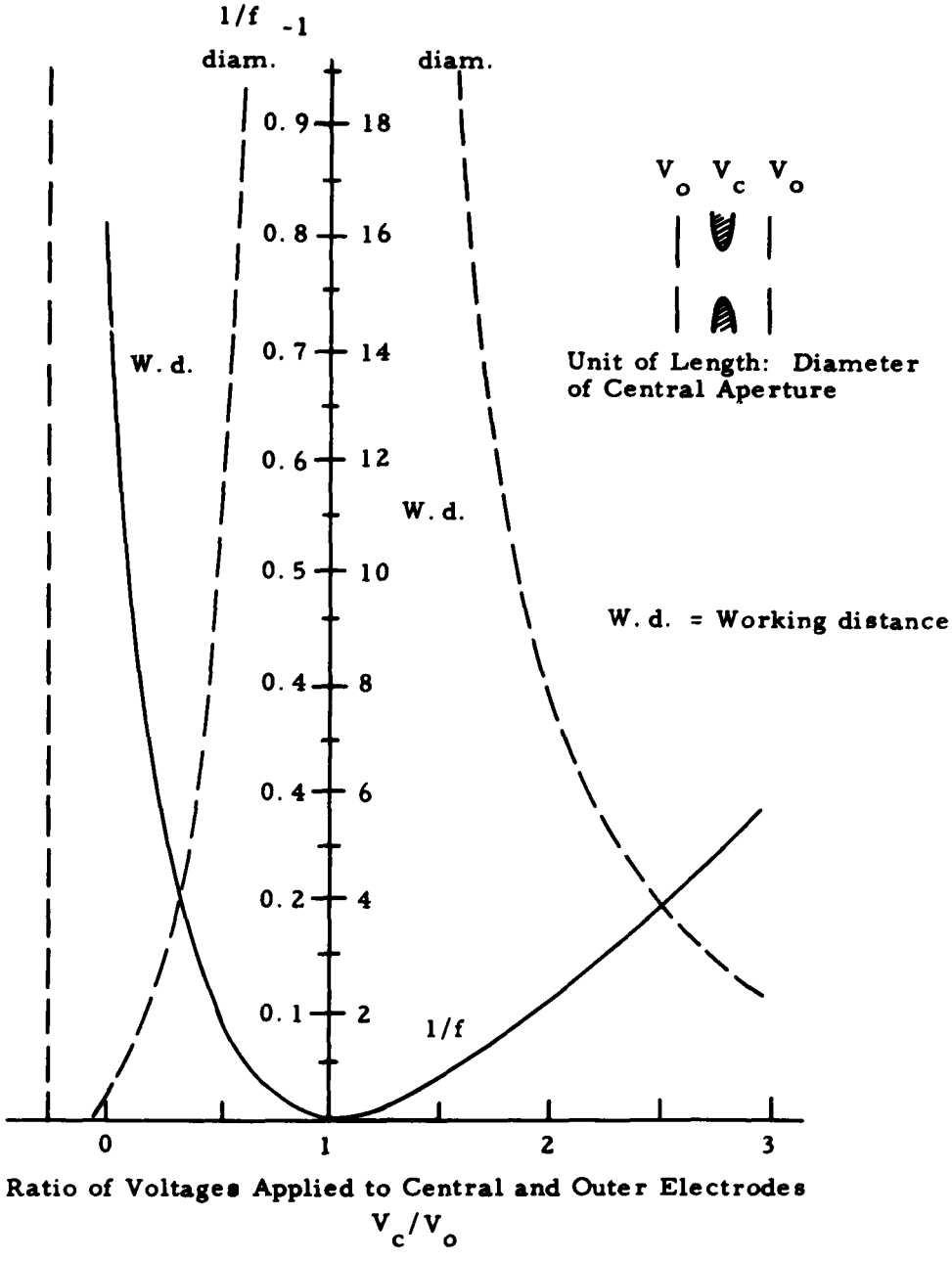

Figure 10. Variations of the Refractive Power and 'Working Distance" with the Ratio of Applied Voltages (after Zworykin[14])

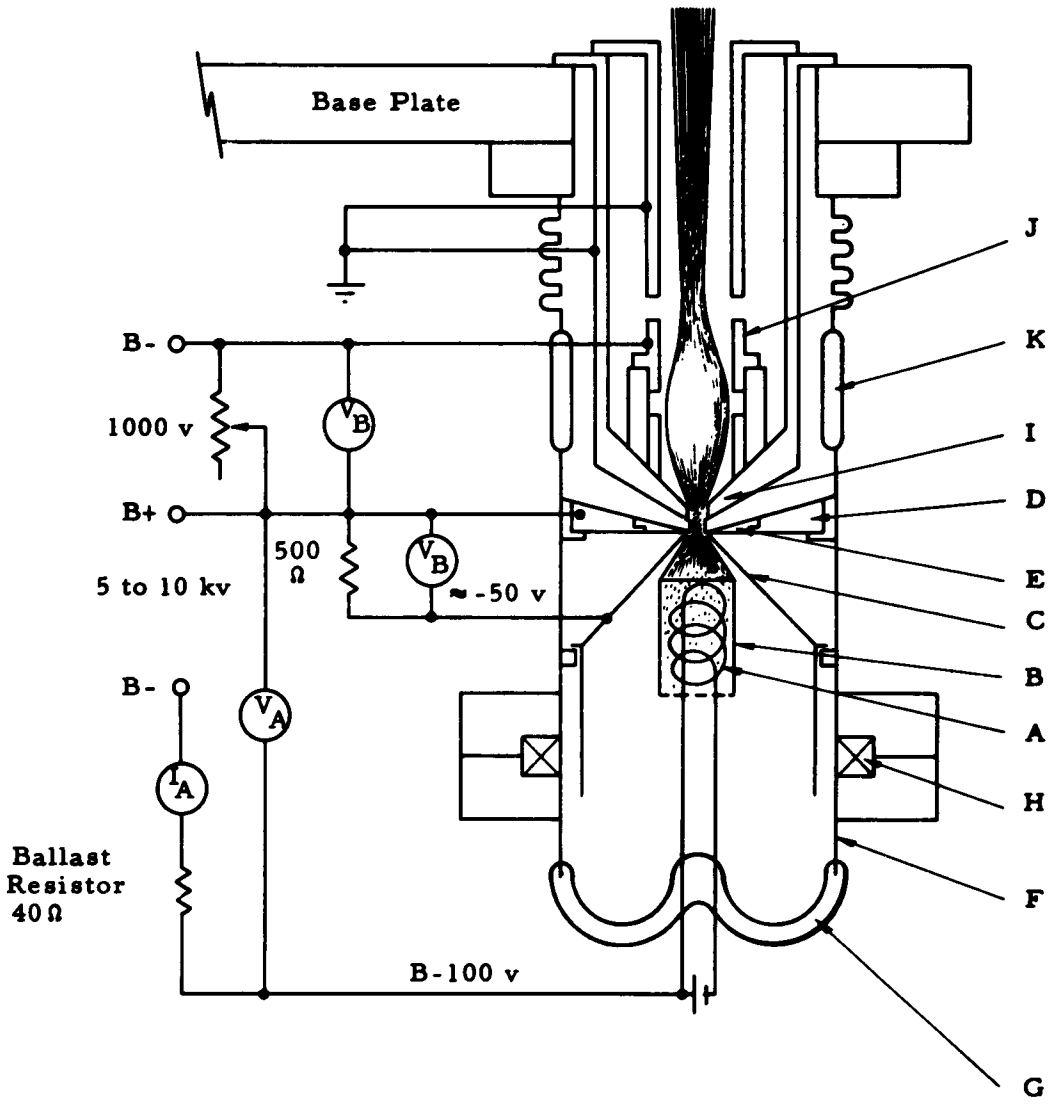

Figure 11. Detail of Unoplasmatron Ion Source and Optical System

Figure 12. Photograph of Unoplasmatron Ion Source

through the anode orifice by kinetic pressure to form a plasma cloud just outside the arc-discharge. Positive ions are removed from this plasma with an electric field applied by the extractor. Until the beam passes through the extractor it is essentially parallel. Because of the lens effect, however, the beam begins to diverge when it leaves the extractor orifice. The diverging beam is collimated by the unipotential lens and enters the vacuum chamber as a parallel beam.

A power-supply system has been developed in this laboratory to operate the unoplasmatron. This system is shown schematically in Figures 13 and 14.

Results of Unoplasmatron Operation

The steps involved in operating the ion beam cleaning apparatus are these: 1) degas the filament, 2) start gas discharge, 3) extract ions from the discharge plasma, and 4) focus ion beam with the unipotential lens.

The first step in operating the unoplasmatron is degassing the tungsten filament. When tungsten wire is fabricated it is usually left with large quantities of occluded gases and vapors (i.e., N_2, CO, CO_2, H_2O, and O_2). Initial degassing of the filament often takes up to 48 hours of heating. This is accomplished by turning up the filament current gradually to 45 amp at 17 v under vacuum, and then pumping off the gases until the discharge chamber pressure drops to about 5×10^{-3} Torr. After the first degassing it is still necessary to bake out the filament whenever the main vacuum chamber is opened, but this can usually be accomplished in about one hour. A residual gas pressure of 5×10^{-3} Torr still indicates some contamination in the discharge chamber. This is flushed out later, however, by the working gas.

The second step is to start the gas discharge. With the filament drawing 45 amp, the anode is set at 200 v, and argon gas is admitted to the discharge chamber. An anode current of about 2 to 3 amp is immediately observed, but this condition is unstable. In order to stabilize the gas discharge it is necessary to reduce the gas flow, whereupon the anode current becomes steady at 1.5 to 2 amp. This is rather high because the maximum current that could be expected from thermionic emission is about 1.13 amp (see Figure 15) for a 1 mm tungsten filament 22.5 cm long.[18]

The additional anode current observed is due to electron multiplication in the working gas. Typical data for experiments of this type by other workers in this field are shown in Figure 16. Here, the logarithm of the anode current when plotted as a function of cathode-anode separation is found to be a straight line for a given field strength and pressure. The physical interpretation of this phenomenon follows:

In traveling from the filament to the anode the emitted electrons will ionize the working gas by electron collision with gas atoms and molecules. If an electron creates α new electrons in a path 1 cm long in the field direction, the increase of electrons dn produced by n electrons in a distance dx will be

$$dn = \alpha n dx \tag{24}$$

$$n = n_o e^{\alpha x}$$

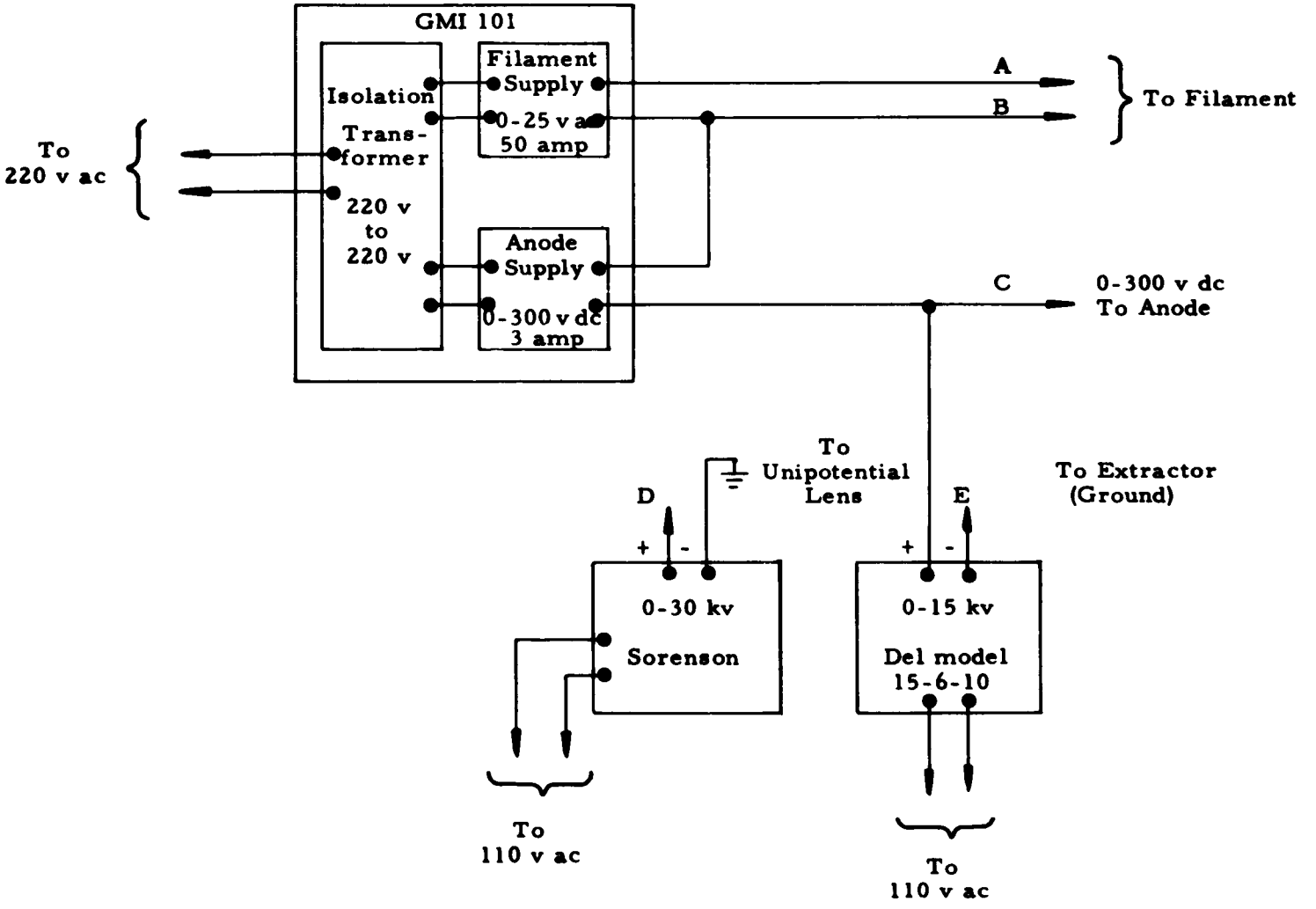

Figure 13. Block Diagram of Power Supplies for Unoplasmatron and Optics

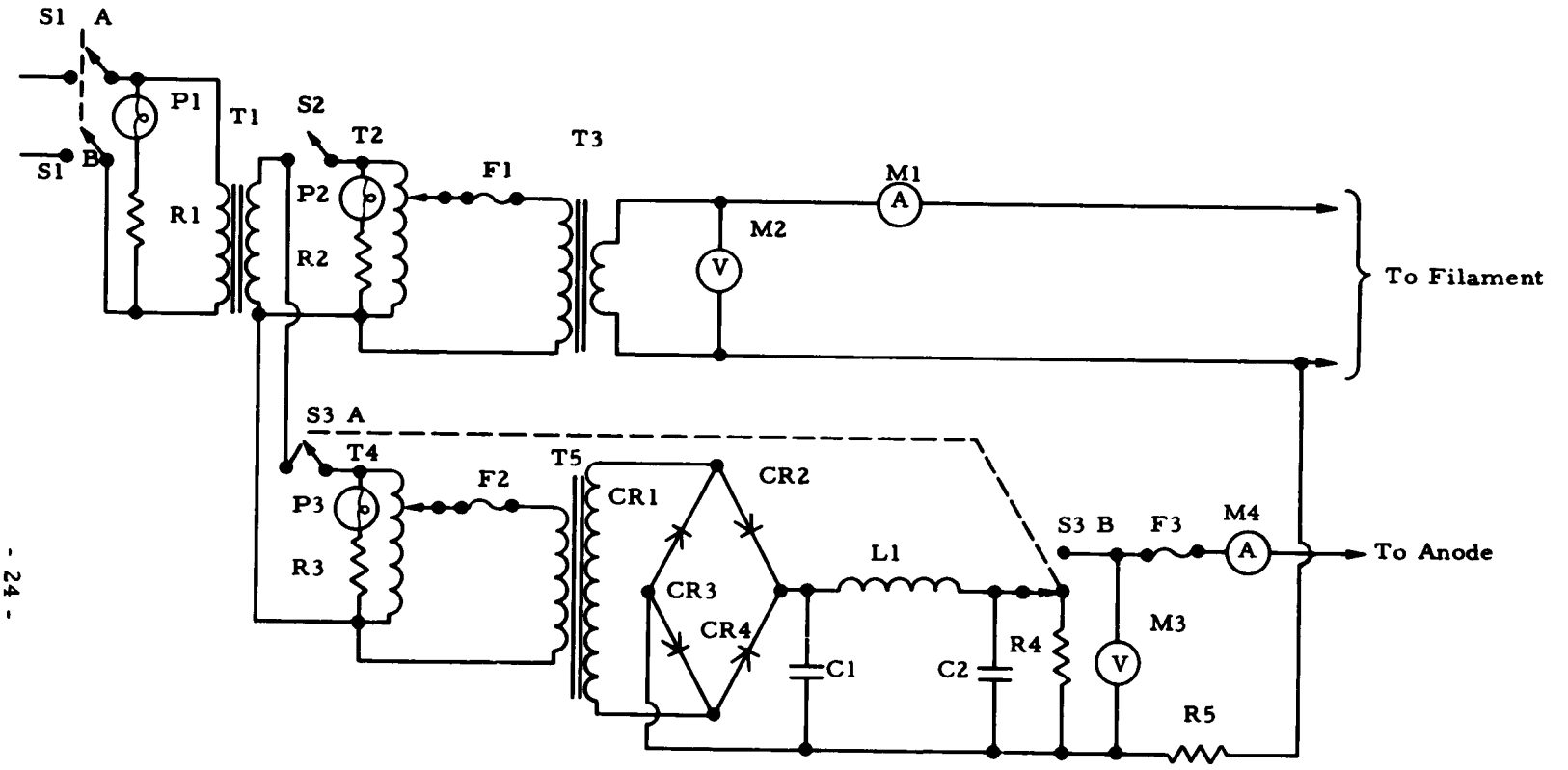

Figure 14. Isolation Transformer, Filament, and Anode Power Supply

C1, 2-80 mfd - 450 v dc
R1, 2, 3 - 82 kΩ - 1/2 w
R4 - 5 kΩ = 30 w
R5 - 3-10Ω - heating element 100 w
T1 - isolation transformer 22 v ac - 220 v ac
T2 - Variac - 220 v - 0-240 v - 5 amp
T3 - filament transformer - 220 v pri - 20 v sec - 50 amp
T4 - Variac 220 v - 0-240 v - 9 amp
T5 - power transformer - 220 v pri - 480 v sec - 1 kva
L1 - choke
P1, 2, 3 - NE 51 pilot light

F1 - 4 amp
F2 - 8 amp
F3 - 3 amp
CR1, 2, 3, 4 - diode rectifier Transitron 1N1347
S1 A & B - switch dpdt
S2 - switch spst
S3 - switch dpdt
M1 - 0-50 amp ammeter
M2 - 0-20 v ac voltmeter
M3 - 0-300 v dc voltmeter
M4 - 0-5 amp dc ammeter

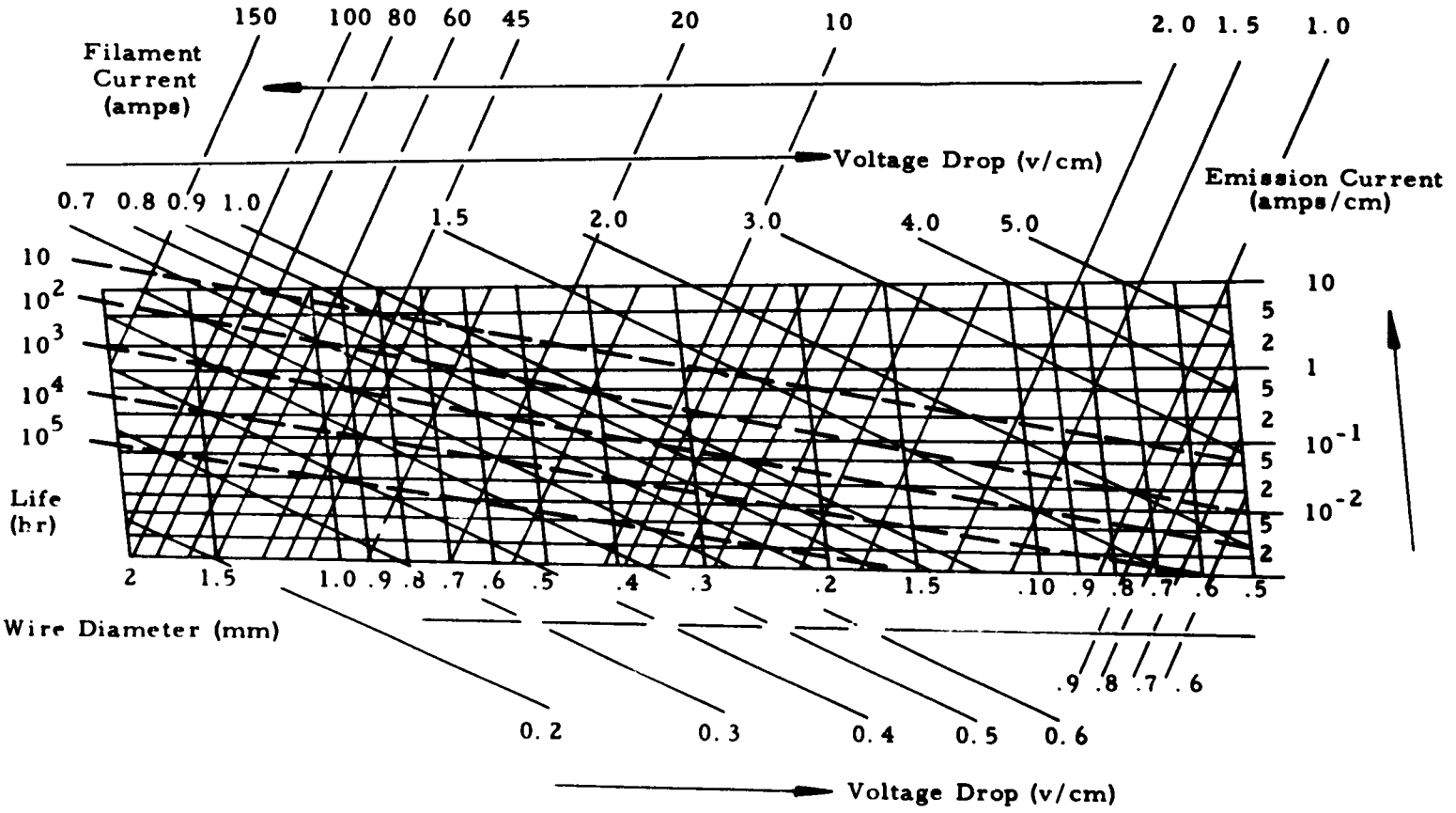

Figure 15. Characteristics of Ideal Tungsten Filaments (after Kohl[18])

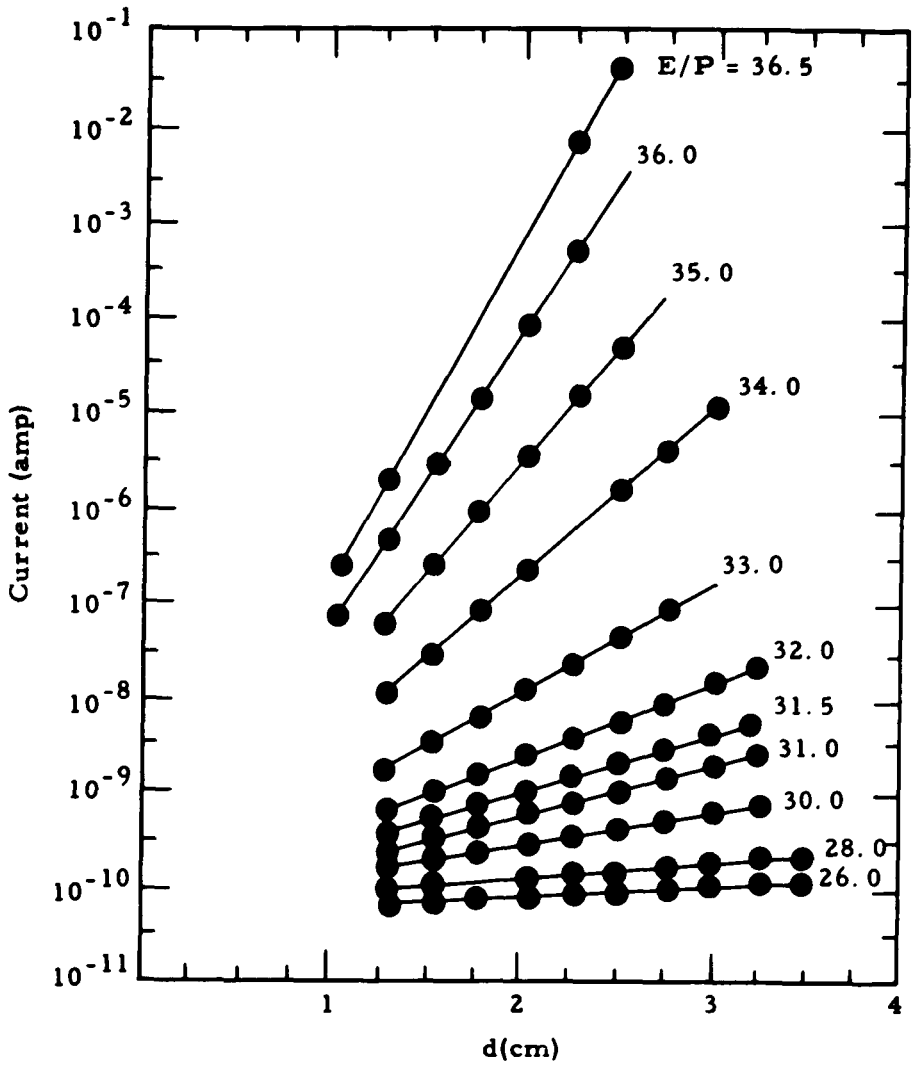

Figure 16. Typical Data for Determining the First Ionization Coefficient (after Brown[19])

where n_o is the initial electron concentration. This corresponds to the observed current determination

$$i = i_o e^{\alpha x}. \tag{25}$$

The quantity α is called the first Townsend coefficient. Although α itself is not a unique function of E/P (field strength/gas concentration), the quantity α/P is. A plot of α/P versus E/P for noble gases is shown in Figure 17. Possibly a more significant coefficient is the ionization produced by an electron falling through a potential difference of 1 v (rather than traveling 1 cm). In this case the current may be written as

$$i = i_o e^{n(V - V_o)}, \tag{26}$$

where V_o is a constant correction factor that is necessary because the energy distribution becomes steady only after the electrons have traveled a certain distance from the cathode. For this case we define the ionization coefficient η which is related to α thus:

$$\eta = \frac{\alpha}{E}. \tag{27}$$

One property of η is that it is itself a function of E/P. Experimental determinations of η as a function of E/P for mixtures of argon and neon are shown in Figure 18. These curves exhibit a maximum for certain values of E/P. The reason for this is that η must be low both at very low pressures (when electrons encounter few atoms) and at high pressures (when elastic energy losses and excitation prevent ionization). Low ionization at high pressure is the cause of the instability noted in the unoplasmatron just after the gas discharge begins.

As shown in Figure 18, η (for constant values of E) is maximum between extremes of high and low pressure; in addition, a small percentage of argon in neon results in a considerable increase in the value of η. This increase is a consequence of the ionization of argon atoms by metastable neon atoms. The effect is greatest at low values of E/P. Strong indirect ionization may thus occur in mixtures of neon and argon, producing much higher values of η than those for pure neon or pure argon. In practical applications advantage is frequently taken of this phenomenon for obtaining low breakdown voltages, which are then only slightly affected by other admixtures.

Once the initial gas discharge has stabilized, the anode current in our unoplasmatron varies as a function of filament temperature and anode voltage as shown in Figure 19. This graph shows the typical limitation of electron current in a hot cathode device both by temperature of the filament (curve AA) and by anode potential. Since no measurable anode current is observed without ionization of the working gas the curves in Figure 19 must also be a complex function of E/P (anode voltage/gas concentration) as illustrated in Figure 18

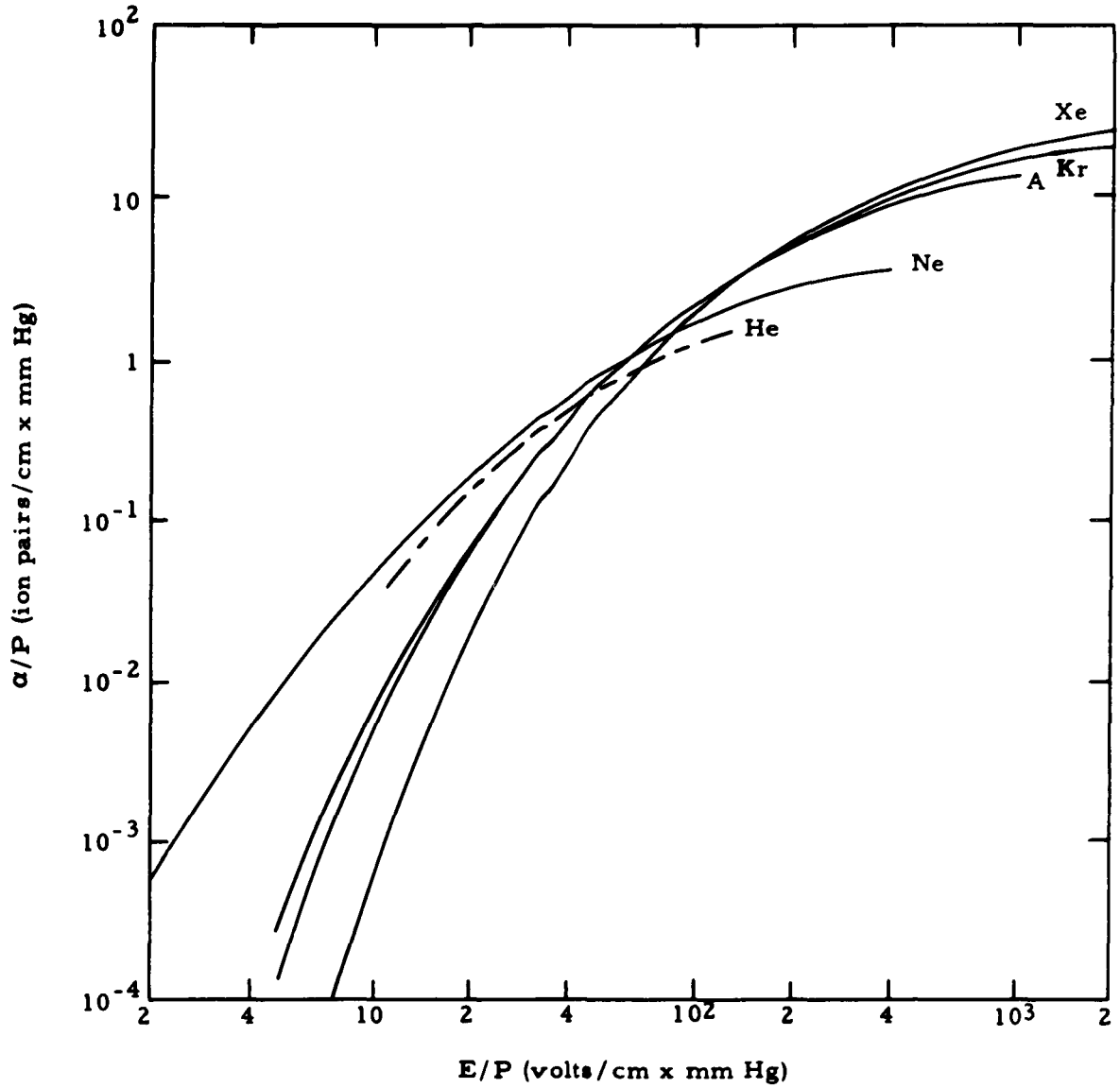

Figure 17. First Townsend Ionization Coefficients in Noble Gases (after A. von Engel[20])

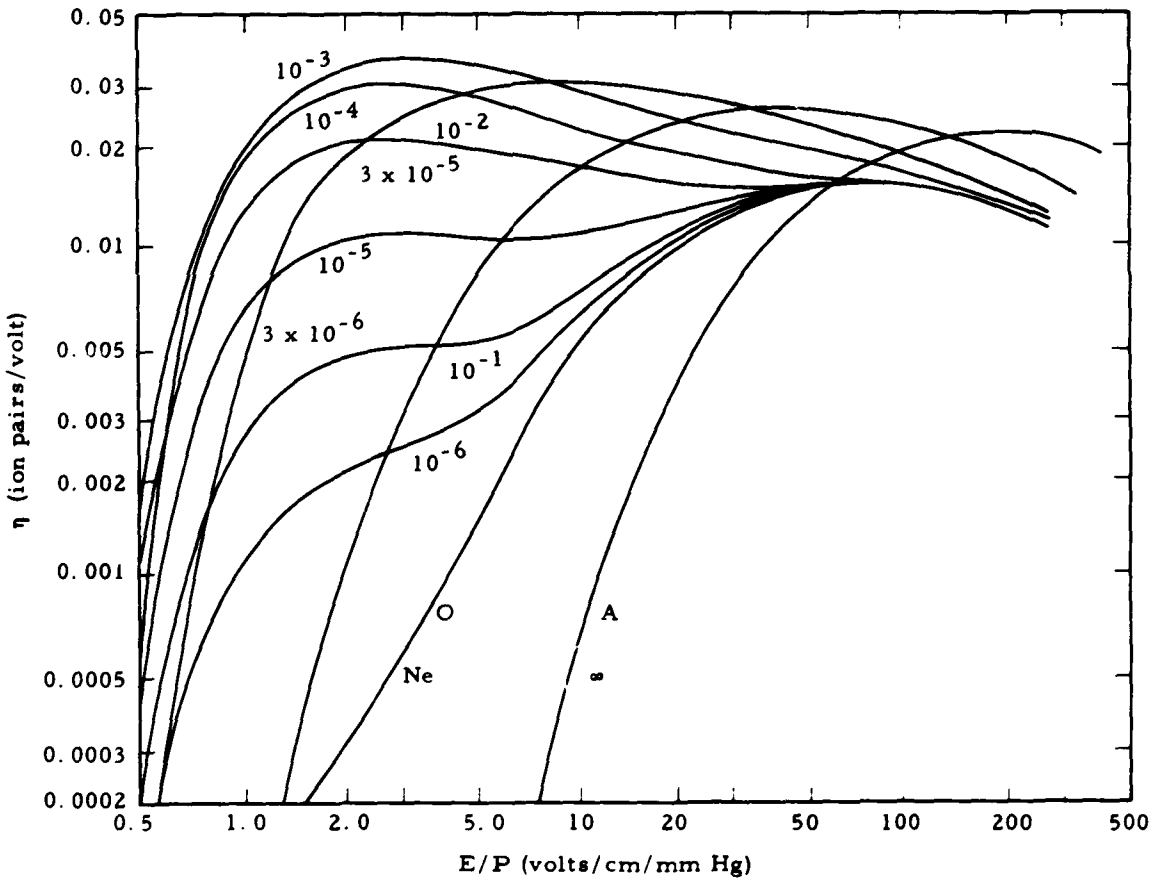

Figure 18. Ionizations per Volt per mm Hg at 0°C for Neon-Argon Mixtures. The Numbers on Each Curve Give the Ratio of the Argon Pressure to the Total Pressure of the Mixture (after Kruithof[21])

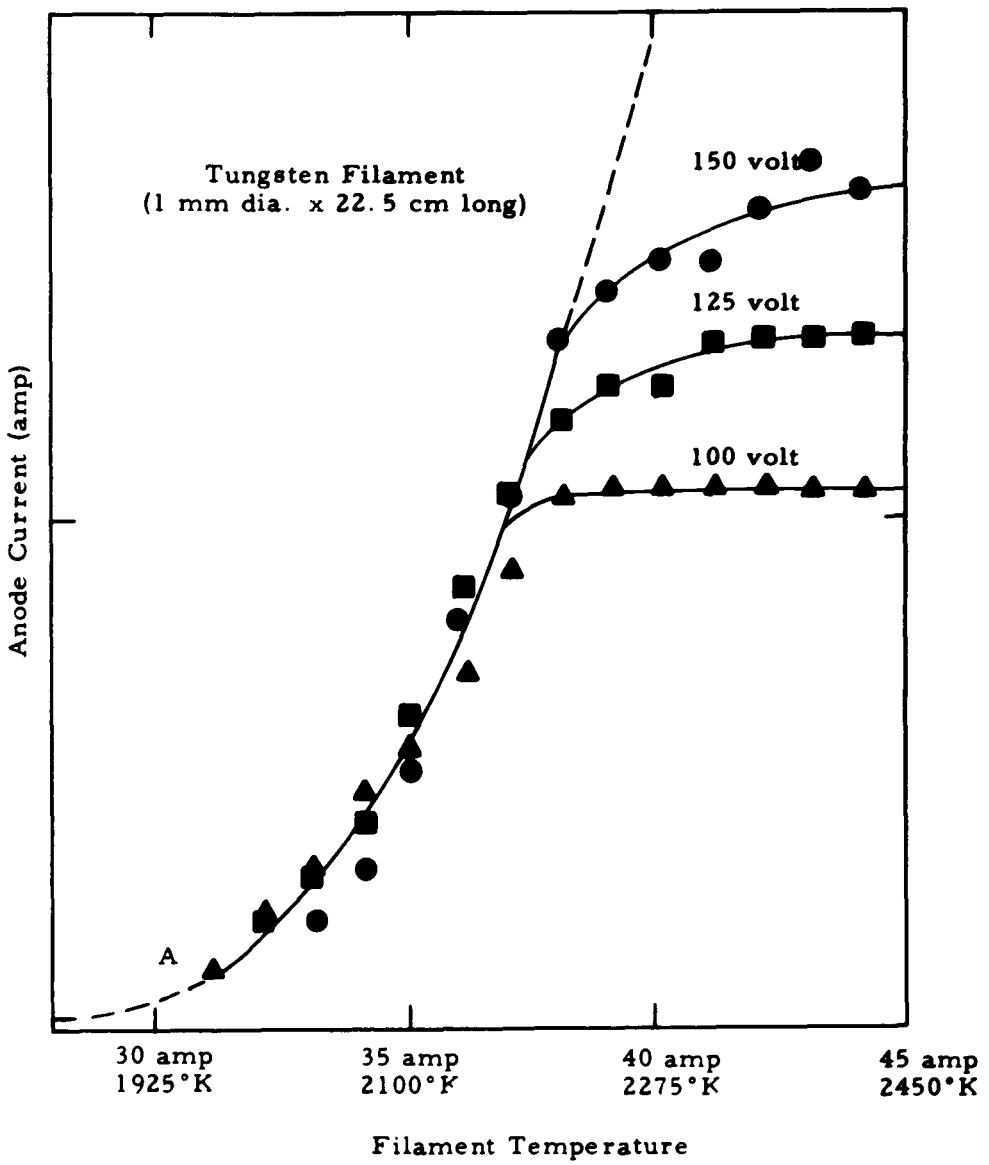

Figure 19. Experimental Curves Illustrating the Relationship between Filament Current, Anode Current and Anode Voltage in an Argon Gas Discharge with the General Mills Designed Unoplasmatron

The third step in operating the unoplasmatron is extraction of ions from the plasma. This is accomplished by turning up the extractor voltage after the plasma has been established. Some of the extracted ions strike the extractor face and are designated extractor current. The rest flow through the extractor orifice striking a target which sits inside the extractor about 4 cm above the extractor tip. The target is placed here only in order to measure the extractor's efficiency. It is removed during the usual operation of the unoplasmatron. Target current data taken as described above are given in Table II

The fourth step in the process is to focus the extracted ion beam with the unipotential lens. This time the specimen itself becomes the target, and the bombarding current measures the efficiency of the unipotential lens. Table III shows typical target current when the unipotential lens is not used. Table IV presents target data obtained when the unipotential lens is used to focus the extracted beam.

In the final analysis, the absolute value of the ion current available for bombardment is not critical. The important thing is whether the ion beam will clean metal surfaces. Experiments in this laboratory have shown that under the right conditions a large, smooth, brightly-etched surface can be produced on copper with the present apparatus. We believe that other metal specimens can be cleaned in the same way.

Table II. Typical Third Step Extractor Current Measurements

Filament Current (amp)	Anode Volt. (v)	Anode Current (amp)	Extractor Volt. (kv)	Extractor Current (μa)	Unipotential Lens Volt. (v)	Unipotential Lens Current (ma)	Target Current (μa)
45	125	.7	10	225	0	0	200
			11	230			225
			12	245			250
			13	265			275
45	150	.9	10	260			175
			11	250			210
			12	260			245
			13	275			275
45	175	1.2	10	350			150
			11	330			180
			12	320			220
			13	320			260
45	200	1.4	10	270			90
			11	320			130
			12	300			160
			13	300	0	0	190

Table III. Bombardment Ion Current without the Unipotential Lens

Filament Current (amp)	Anode Volt. (v)	Anode Current (amp)	Extractor Volt. (kv)	Extractor Current (μa)	Unipotential Lens Volt. (v)	Unipotential Lens Current (ma)	Target Current (μa)
45	125	.8	10	215	0	0	28
			11	230			36
			12	245			45
			13	255			52
45	150	1.2	10	220			23
			11	225			31
			12	235			38
			13	250			46
45	175	1.5	10	240			18
			11	250			23
			12	250			30
			13	270			37
45	200	1.8	10	210			14
			11	230			19
			12	260			25
			13	260	0	0	31

Table IV. Bombarding Ion Current with the Unipotential Lens Used for Focusing

Filament Current (amp)	Anode		Extractor		Unipotential Lens		Target
	Volt. (v)	Current (amp)	Volt. (kv)	Current (μa)	Volt. (kv)	Current (μa)	Current (μa)
45	125		10				
			11				
			12	450	6.45	.05	42
			13	475	7.0	.05	36
45	150	.9	10				
			11	345	7.0	.07	84
			12	340	7.8	.07	87
			13	360	7.8	.08	78
45	175		10				
			11				
			12				
			13				
45	200		10				
			11				
			12				
			13				

(blanks indicate no data available)

PART II

TECHNIQUES FOR SURFACE ENERGY MEASUREMENTS

Unsatisfied valence forces at the surface of a metal lead to a state of tension in the surface atoms and to compression of those underneath. These forces also account for adsorbed films of substances bonded to the metal surface in varying degrees. Films with low bonding energy are physically adsorbed, and films with high bonding energy are chemisorbed. Two good methods of studying the degree of coverage and the effect of surface films are friction measurements and contact potential measurements.

FRICTION MEASUREMENTS

Adsorbed gases and vapors are largely responsible for the easy sliding of one metal over another at light loads, the coefficient of friction varying from 0.5 to 1.0. The coefficient of friction between metals relatively free of surface films is increased by a factor of 6 to 12; if pure surfaces are placed together, immediate seizing occurs.[22] If polarorganic compounds are physically adsorbed (or, better, chemisorbed) on these surfaces, the coefficient of friction is appreciably reduced. The important films in this process are either one or at most a few molecules thick.[23]

A light-load friction apparatus designed and constructed after the method of Whitehead[24] has been in use in this laboratory for over 3 years (Figure 20). The sliding surfaces consist of a metal sample (A) mounted on a glass turntable (B), and a hemispherically-tipped slider (C) mounted at one end of the spring steel wire (D). The other end of the wire is clamped to a U-shaped beam (E), which is supported by a cantilever spring (F). The normal load on the slider is applied by raising the end of the U-beam a known distance with a micrometer (G), thereby bending the wire in a vertical plane.

When the turntable is rotated slowly, the slider is dragged along with the specimen, bending the wire until the restoring force equals the static friction force. Deflection of the wire, which corresponds to the friction force, is detected and recorded by an electromechanical transducer. The needle (H) contacts and moves with the wire (D), rotating the coil (J) in a field of constant magnetic flow created by supplying the coil (K) with a low-voltage, high-frequency power source. The magnitude of the emf induced in the rotating coil is proportional to its position in the magnetic field. This emf is amplified and recorded continuously on an oscillograph chart. The transducer is calibrated by using a micrometer to deflect the wire a known distance.

This apparatus has been used extensively at General Mills for studies of thin oxide films and monomolecular films of organic compounds on metals.[23]

Recently, the friction apparatus was modified as shown in Figure 21. The friction probe is now used in an inverted position to better accommodate the ion-beam cleaning technique.

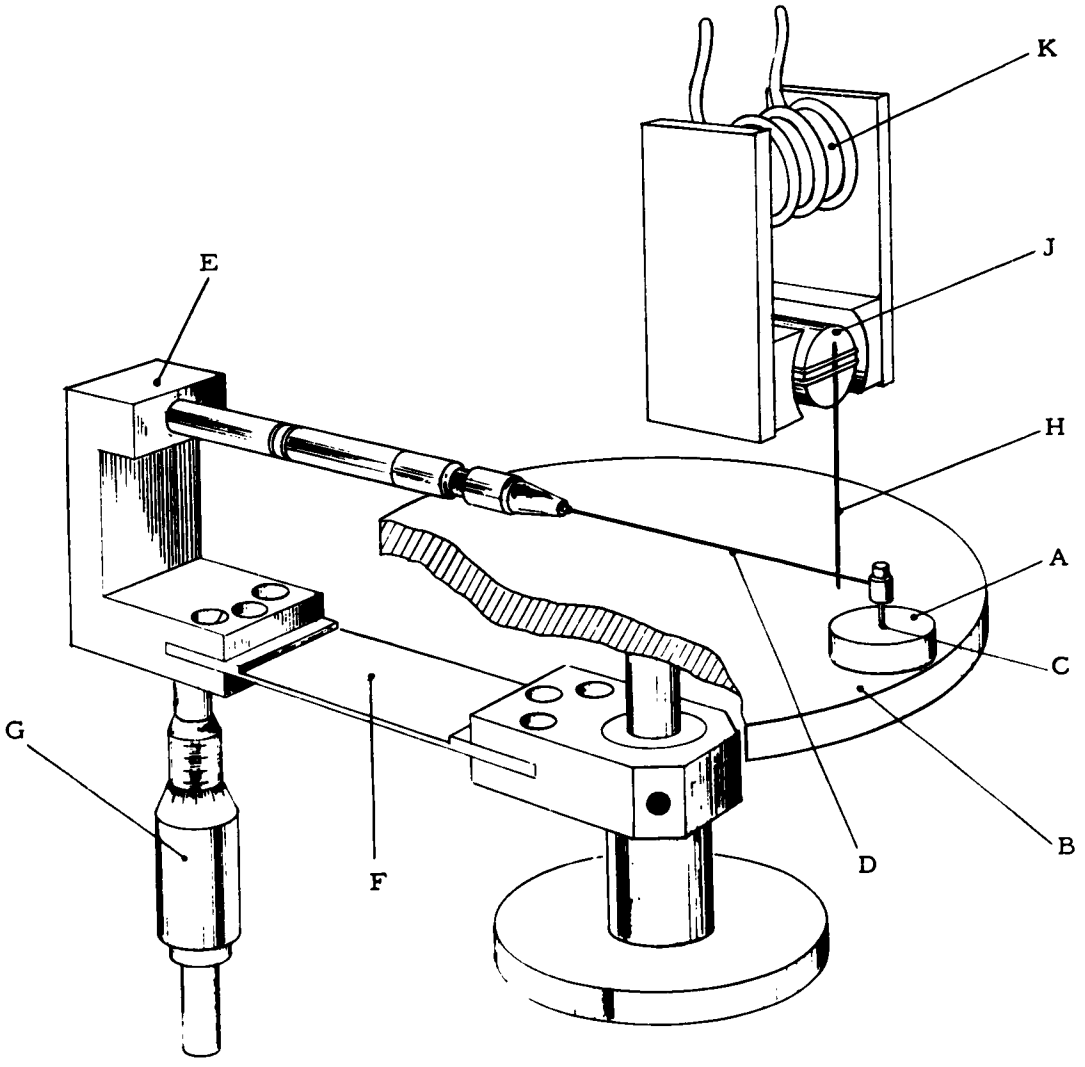

Figure 20. Friction Apparatus

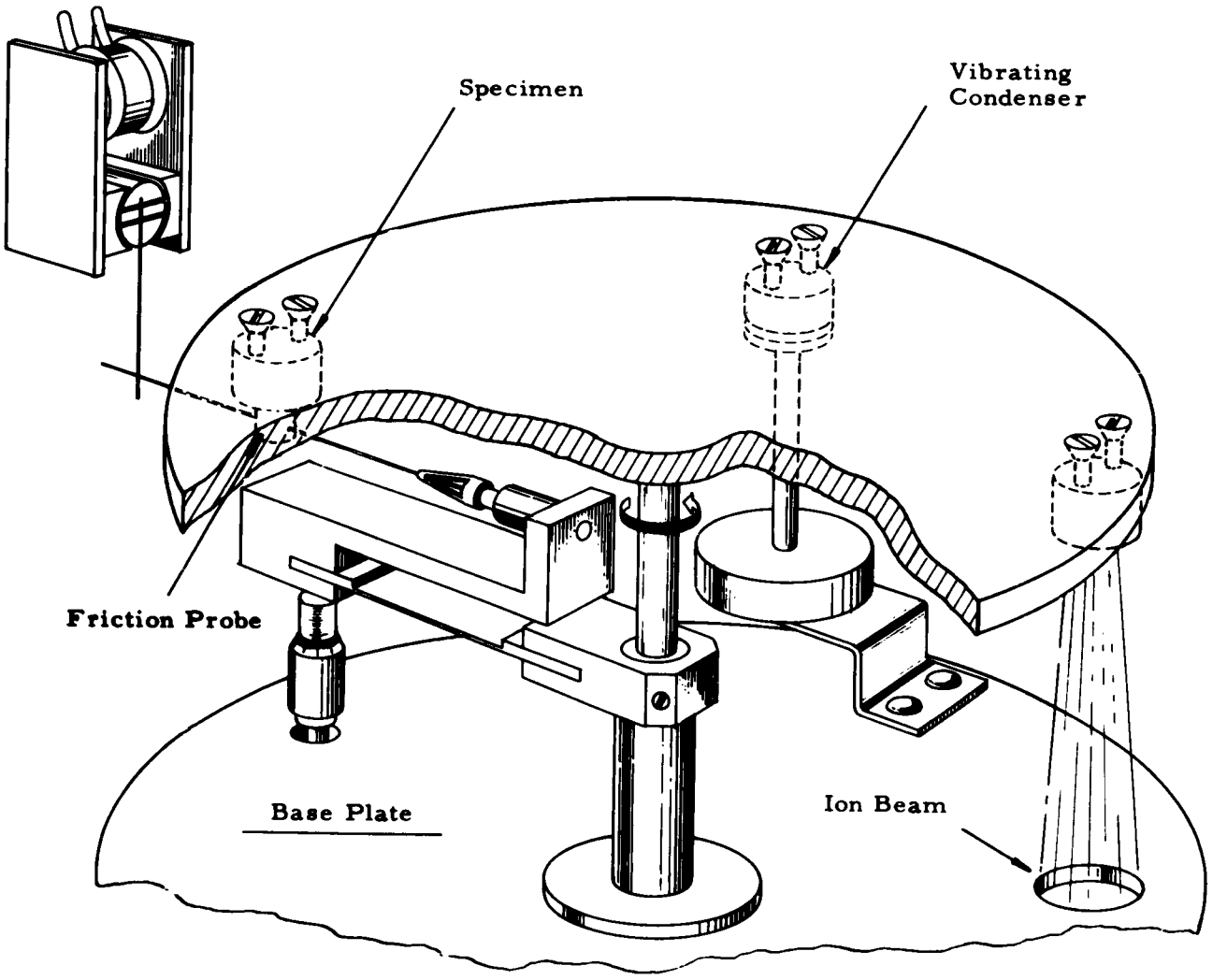

Figure 21. Modification of the Experimental Apparatus

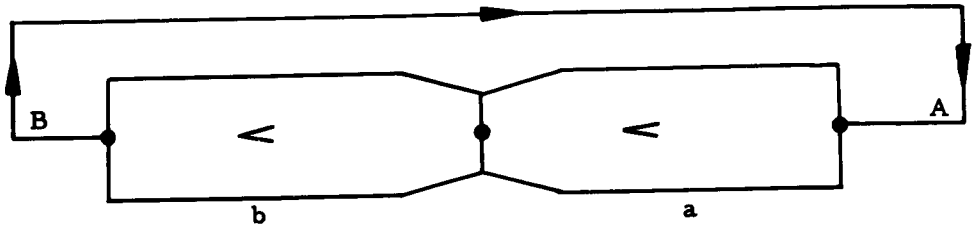

Figure 22. Illustration of Contact Potential

CONTACT POTENTIAL MEASUREMENT

Theory

Contact potential difference is defined as the difference in work required to remove an electron from the interior lattice of each of two solids in contact to an external point at zero potential. Experiments show that a definite amount of work ϕ must be done against electrical forces in carrying an electron from the interior to the surface of a conductor. This quantity is called the work function.

Assume that two conductors (a) and (b) (Figure 22) are placed in contact. If a unit positive charge is carried around the closed path indicated in the figure, the total electrical work is zero because the forces are electrostatic. Let V_{ab} be the potential drop, if any, from point (A) just outside the surface of conductor (a) to point (B) just outside the surface of conductor (b). The work equation is

$$\frac{\phi_a}{e} - \Pi_{ab} - \frac{\phi_b}{e} - V_{ab} = 0 \qquad (28)$$

where ϕ_a = work function of conductor (a)
ϕ_b = work function of conductor (b)
Π_{ab} = Peltier coefficient
V_{ab} = contact potential difference
e = charge of the electron (negative quantity).

The Peltier coefficient Π_{ab} appears with a negative sign since the electric field to which it refers is in the direction opposite to the Peltier emf. Since

the contact potential difference is about 4 magnitudes greater than the Peltier emf, the Peltier coefficient is usually ignored, and Eq (28) is written[25]

$$V_{ab} = \frac{\phi_a - \phi_b}{e} . \tag{29}$$

When a metal is covered with a surface film, the distribution of electrons and positively-charged particles on the surface depends on the relative affinity of the positive ions of the metal and the atoms of the surface film for electrons. In general, an additional double layer is produced by the surface film. If this has the negative side outward, it increases the work of extracting electrons; if the positive side is outward, the work of extraction is decreased. The most commonly-occurring gas films decrease the emission, increasing the work function.[26]

There are four principal methods for measuring contact potential:[27] 1) condenser method, 2) ionization method, 3) photoelectric method, and 4) thermionic method. The oldest and in many ways the best method of measuring contact potential is the condenser method.

In Figure 23 a condenser is formed by the two surfaces where (a) is the reference surface and (b) the experimental surface. A potential difference V_{ab} will exist between the surfaces, and each condenser plate will carry a charge expressed by

$$Q = CV_{ab} \tag{30}$$

where C is the capacitance of the condenser. If the distance between (a) and (b) is changed, C will change and cause Q to change. The galvanometer (G) will detect a flow of charge. If a potential difference equal and opposite to V_{ab} is introduced through the voltage divider, the potential of plate (a) will be made the same as that of (b), Q will be zero, and movement of plate (a) will cause no current to flow through (G). The voltmeter (V) will then measure V_{ab} directly.

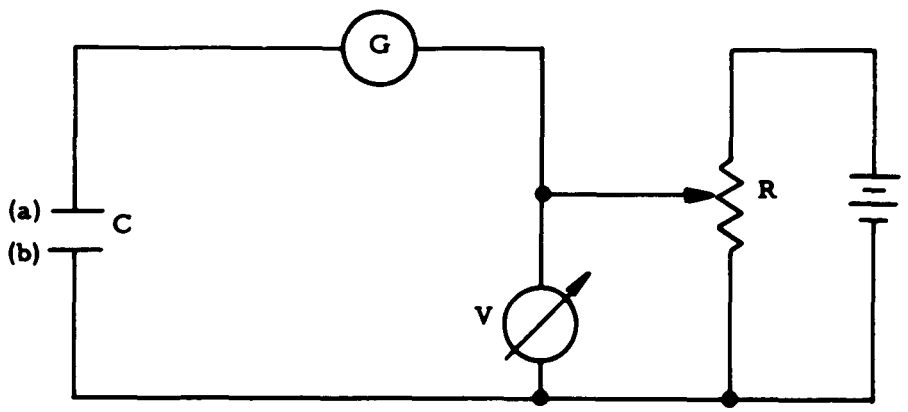

Figure 23. Condenser Method

The principal problem associated with the condenser method is the need to separate the plates. Originally the methods were rather crude. Kelvin,[28] for example, merely separated the plates by hand.

A great improvement on the Kelvin method was introduced by Zisman.[29] In this technique one plate of the condenser is caused to vibrate harmonically with respect to the other. Then an alternating current flows in the resistor (R) which connects the metals. The magnitude of the voltage drop across (R) is a direct measure of the contact potential. The following analysis of the vibrating condenser apparatus is offered by Bewig.[30]

In Figure 24, (C) represents a vibrating condenser formed by two metals, (V) represents the resulting contact potential, and (E) is an external battery of opposing polarity.

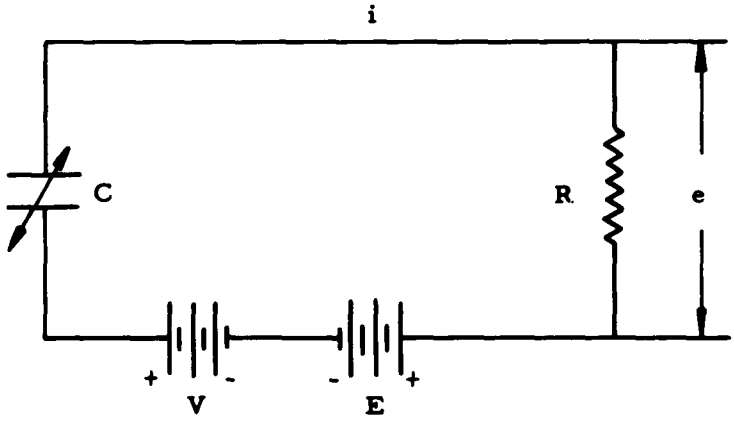

Figure 24. Diagram of the Vibrating Condenser Contact Potential Difference Apparatus

Assuming that C varies harmonically with time,

$$C = C_o + C_1 \sin \omega t \tag{31}$$

and then

$$(V-E) - R_i = \frac{1}{C}\int i\,dt. \tag{32}$$

This equation has a solution of the form

$$i = \frac{(V-E)\,C_1}{C_o\sqrt{\left(\frac{1}{\omega C_o}\right)^2 + R^2}} \sin(\omega t + \phi_1) - \frac{(V-E)\,C_1^2 R}{C_o^2\sqrt{\left[\left(\frac{1}{\omega C_o}\right)^2 + 4R^2\right]\left[\left(\frac{1}{\omega C_o}\right)^2 + R^2\right]}}$$

$$\sin(2\omega t = \phi_1 - \phi_2) + \text{higher orders of } C_1/C_o, \tag{33}$$

where ϕ_n is a phase term.

If C_1, the maximum incremental change in the capacity due to the harmonic vibration, is small compared to C_o, the quiescent value of the capacity, the approximate solution (multiplied by R to give e) becomes

$$e = iR \approx \frac{(V-E)\,\omega C_1 R}{\sqrt{1 + (\omega C_o R)^2}} \sin(\omega t + \phi_1). \tag{34}$$

From Eq (34) it is evident that e will disappear when E = V. The magnitude of e as it varies through the null point should be as large as possible for the most accurate determination of the null. This voltage is directly proportional to ω, C_1, and R. Since e increases with frequency ($\omega = 2\pi f$), and since C_1 is maximum at the fundamental resonant frequency of the mechanical vibrating system, the resonant frequency determines both ω and C_1. The resistance R should be approximately equal to the quiescent capacitive reactance of the condenser ($1/\omega C_o$).

The area of the vibrating condenser plates should be small because homogeneous metal surfaces are difficult to prepare, and small-area plates are aligned more easily. The distance between the plates is limited by the fringing field. The contribution of the fringing field on the edges and back surfaces of the condenser

to the measured contact potential difference depends on the metals used, on their crystal structure and orientation,[31,32] on adsorbed gases, and on the cleanliness of the surfaces.[33,34]

The formulas for computing the capacitances of circular electrodes with and without a fringing field are as follows:[35]

$$C_n = \frac{1.113D^2}{16d} \quad \mu\mu f \tag{35}$$

where D = diameter of plates

d = distance between plates.

The added capacitance due to the fringing field is

$$C_e = \frac{1.113D}{8\pi}\left[\ln\frac{8\pi D}{d} - 3 + Z\right]\mu\mu f \tag{36}$$

where $Z = (1 + t/d)\ln(1 + t/d) - t/d \ln t/d$

t = plate thickness

D, d, and t are in centimeters.

Evidently, the work functions of the edges and back surfaces of the two metal plates are different from those of the inner faces. This causes a variation in contact potential as a function of the distance between the plates. Bewig[30] found that for plates 1 cm in diameter and 0.1 cm thick the measured contact potential varied over 100 percent when d changed from 0.04 cm to 0.10 cm. In contrast, he also found that the contact potential varied less than 5 percent when d was smaller than 0.04 cm.

Experimental Design

The contact potential apparatus designed for our system is a modification of the of the apparatus discussed by Bewig.[30] The apparatus is shown schematically in Figure 25. The functional parts of the device are the vibrator and the reference plate. The vibrator provides harmonic motion to one condenser plate. It is composed of a steel housing (A) (Figure 25), a pair of electromagnetic coils (B), a thin, circular steel plate (C), and a vertical shaft (D). The stainless steel housing (A) provides a shielded container for the coils. The coils (B) are wound unpotted on Teflon forms. The stainless steel plate (C) acts as a vibrating surface. The housing and plate are made of No. 416 stainless steel because this material has a relatively high magnetic permeability and low retentivity in addition to being noncorrosive. The shaft (D) is made of nonmagnetic No. 304 stainless steel. In essence, the vibrator is an electrically and magnetically shielded earphone that is compatible with a very-high-vacuum system.

The reference condenser plate (E) serves as a stable reference for the surface under investigation. The plate is a thin disc of platinum about 0.75 inch in

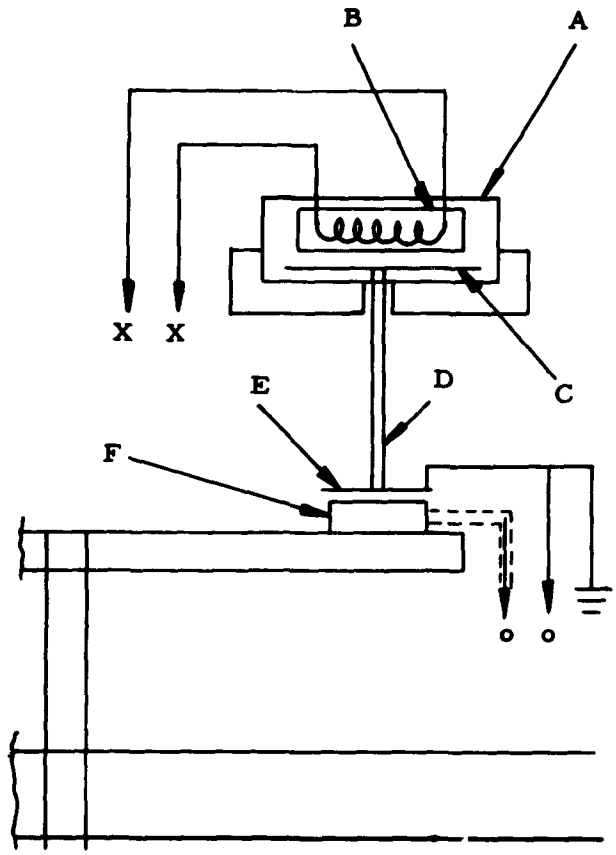

Figure 25. Contact Potential Apparatus

diameter attached to the end of the vibrator shaft. It is necessary that the condition of the vibrating surface vary much less than the surface under investigation in a limited range of conditions. Therefore, a noble metal such as platinum is a good choice for the reference surface. Stable reference electrodes of noble metals coated with a thin film of FEP Teflon resin have recently been developed for the measurement of contact potentials in gases and vapors.[36]

In operation, the surface (F) under investigation is moved into position below the reference plate (E). The gap between the two surfaces is preset. The reference plate is then vibrated with the earphone which is driven by an audio oscillator (refer to Figure 24). An alternating current will flow through the resistor (R) until the contact potential difference (V) has been balanced by a back emf from the battery (E). An oscilloscope is used to determine the null condition and a voltmeter is used to read the contact potential directly. The contact potential circuit is shown in Figure 26.

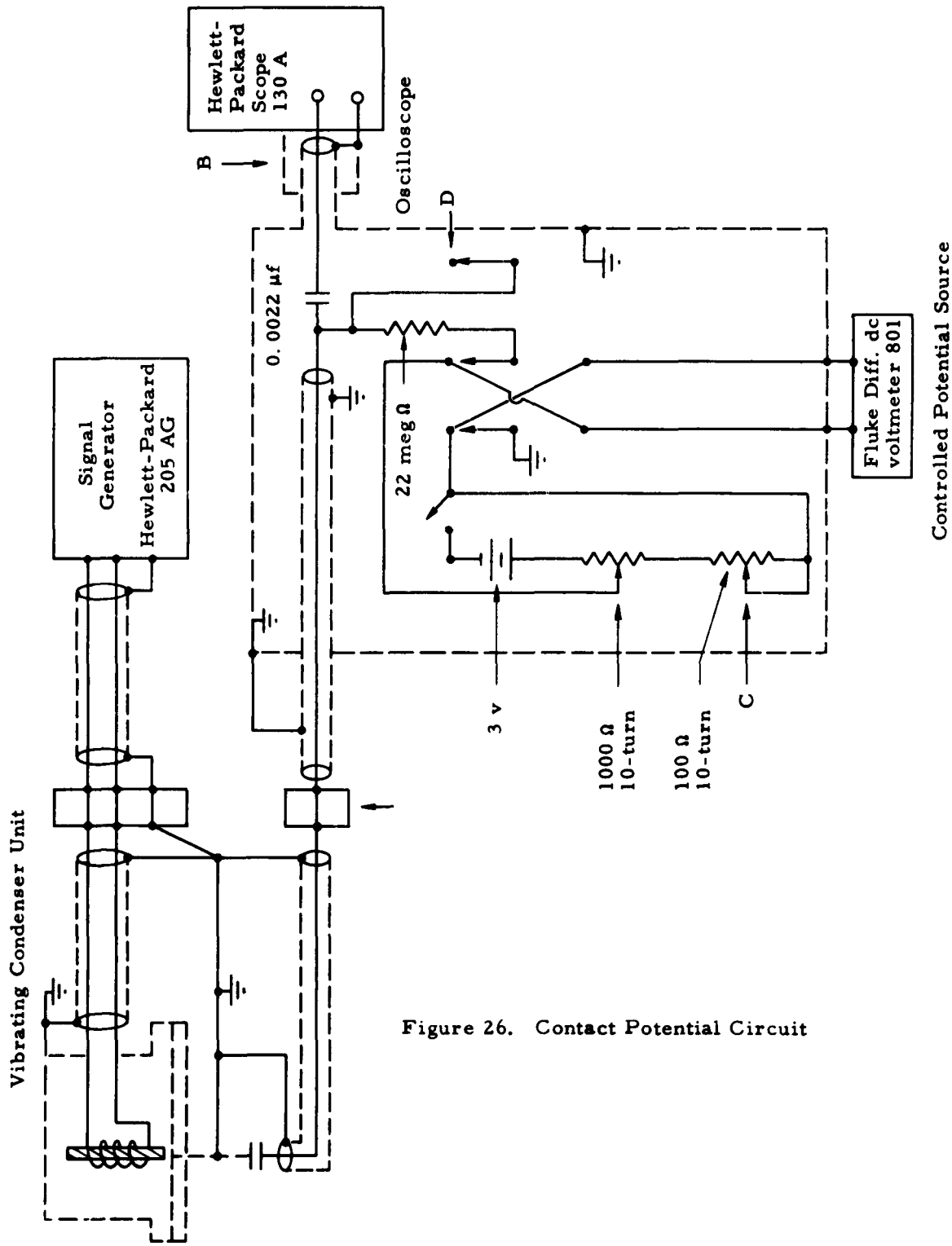

Figure 26. Contact Potential Circuit

EXPERIMENTAL RESULTS

In operating the contact potential apparatus, technique was found to be as important as electrical shielding in reducing background. Although it is not specified in the literature, we found that attaching the signal lead to the immovable sample rather than to the vibrating plate was much more satisfactory. With the signal lead coming from the specimen, both extraneous voltage and signal distortion were greatly reduced. In order to reduce background noise it was found necessary to completely isolate the signal lead feedthrough (Figure 26A) from the other leads. This was accomplished by bringing the signal lead into the chamber through a separate high-voltage feedthrough. All other vibrating condenser leads enter the chamber through a standard instrumentation or cluster feedthrough. In addition a grounded enclosure at (B) produces a further reduction in extraneous background voltage. When these precautions were taken, the extraneous background voltage measured about 0.2 mv peak to peak. Two other modifications include a 100 ohm potentiometer at (C) for fine adjustment of potential and a grounding switch at (D) to bleed off electrostatic charges which might accumulate during sputter cleaning.

As shown by Eq (34), the sensitivity e of the contact potential apparatus is a function of the excitation frequency. A plot of sensitivity versus frequency for our apparatus is shown in Figure 27. The resonant frequency was found to be about 285 cps. As stated earlier, Bewig[30] found that plate separation distance had a marked effect on the measured contact potential. We were not able to verify his data since we did not have reproducibly clean surfaces. However, the sensitivity of the apparatus was found to be very dependent on plate separation. As shown in Figure 28, sensitivity falls off rapidly as plate separation increases. Our apparatus workes well with a plate separation of about 0.1 mm, which is well within the limits established by Bewig.[30]

Some measurements have been made of the contact potential of metal surfaces in air. The contact potential of a polished polycrystalline titanium surface relative to platinum was found to vary from about 0.32 v to 0.42 v, depending on how well the surfaces were cleaned. The standard method for cleaning such surfaces in air has been to swab the specimen on a kitten's-ear cloth immersed in distilled water until they hold a stable water film over the whole surface after emersion. Evidently these surfaces become cleaner the longer they are swabbed, although the water test is not sensitive to the difference. A polycrystalline copper surface cleaned in this manner measured about 0.17 v relative to platinum. It is difficult to verify such results since very little data exist in the literature. However, in the International Critical Tables[37] there is a brief table of contact potential measurements on copper and platinum versus brass obtained by the vibrating condenser method. These data are shown in Table V. From this table it is possible to compare indirectly the contact potential of copper versus platinum in air in the following way:

$$(V_{Cu} - V_{brass}) = -0.15$$

$$-(V_{Pt} - V_{brass}) = -0.32$$

$$V_{Cu} - V_{Pt} = +0.17$$

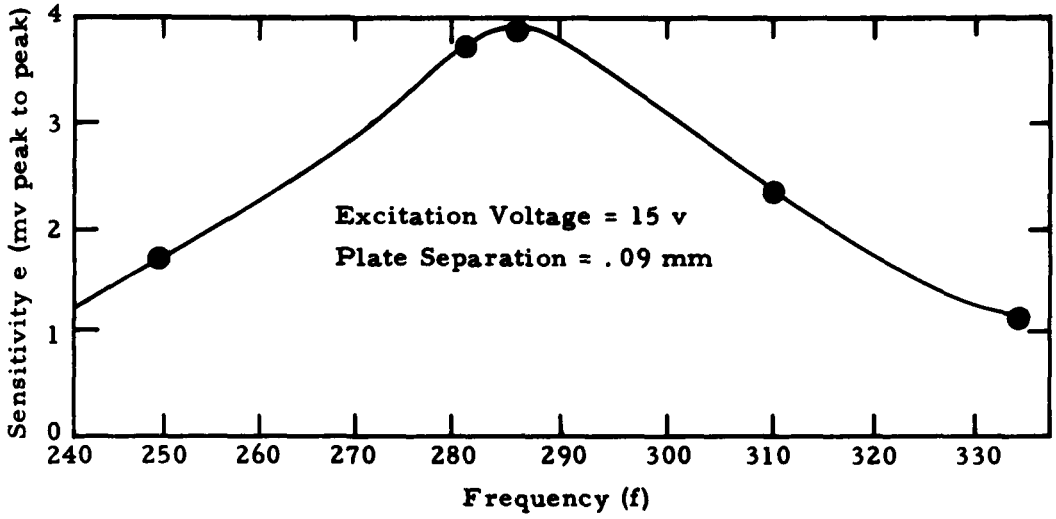

Figure 27. Plot of Sensitivity (e) versus Frequency (f)

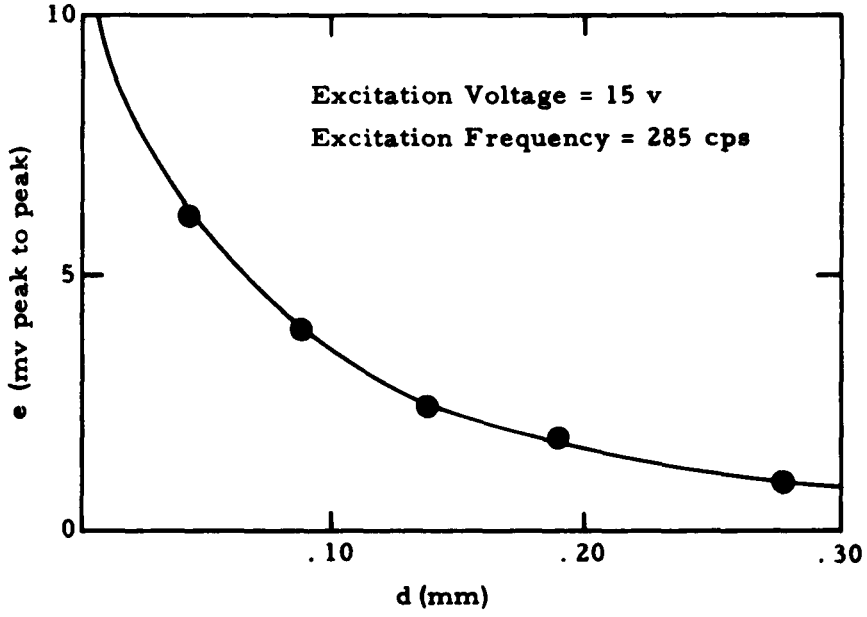

Figure 28. Plot of Plate Separation (d) versus Sensitivity (e)

This result compares favorably with the value determined in our laboratory. The contact potential of metal surfaces changes rapidly in air. Figure 29 shows the change of contact potential versus time for a cleaned polished titanium surface in air. This demonstrates why it is so hard to obtain reproducible measurements in air. At present the accuracy of the measurements is believed to be about ±5 mv.

In addition to the above measurements, the contact potential apparatus has been operated in a vacuum of 10^{-5} Torr, and it performed satisfactorily.

Table V. Contact Potential of Copper and Platinum versus Brass-Vibrating Condenser Method[37]

	$V_{metal} - V_{brass}$	
	Cu	Pt
Surface freshly scraped	+0.10	
Four days after scraping	-0.110	
Before scraping	-0.106	
Air at atmospheric pressure	-0.04	-0.30
Air at 1×10^{-4} mm Hg	-0.04	-0.28
Highest value after heating to high temperature in vacuum	+0.44	-0.23
In air at atmospheric pressure	-0.15	-0.32
In air at room temperature and atmospheric pressure	-0.154	-0.354

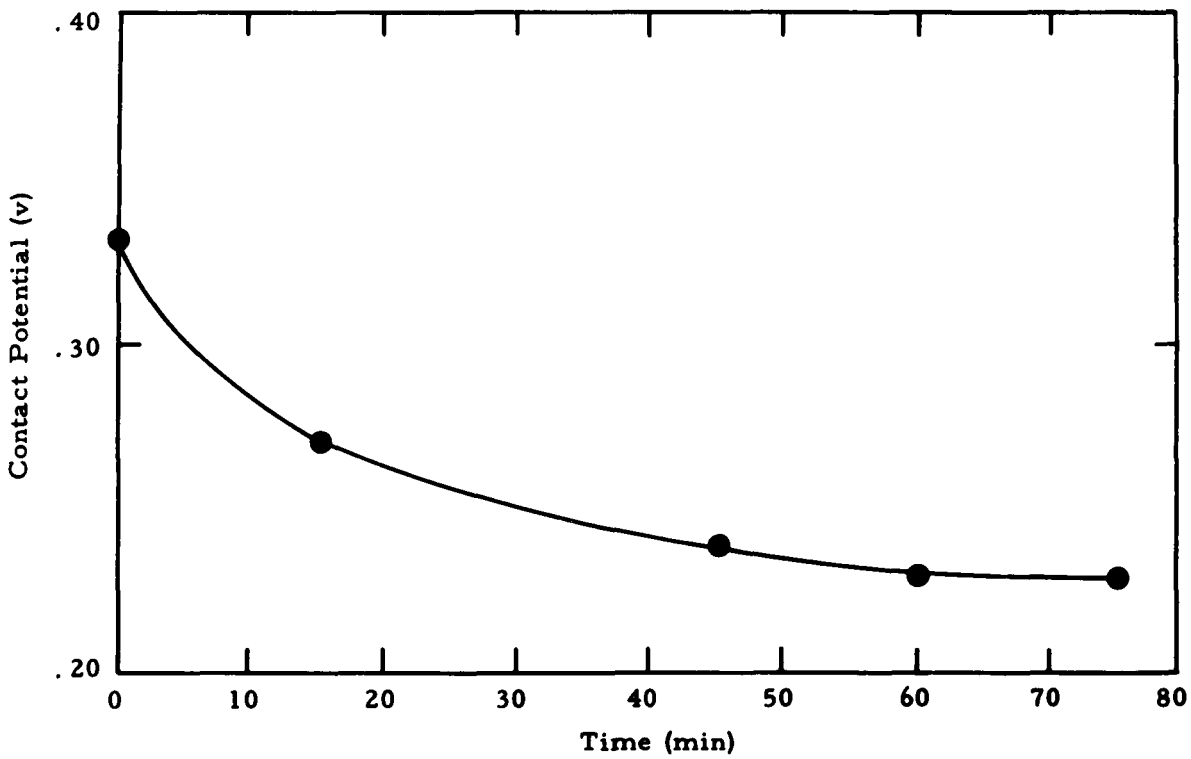

Figure 29. Contact Potential versus Time for a Freshly Cleaned Titanium Surface in Air

REFERENCES

1) Bowden, F. P. and D. Tabor. The friction and lubrication of solids. Oxford, Clarendon Press, 1950.

2) Schlier, R. E. and H. E. Farnsworth. "Structure and adsorption characteristics of clean surfaces of germanium and silicon." J. Chem. Phys. 30: 917-26 (1959).

3) Wehner, G. K. "Sputtering by ion bombardment." In: Advances in electronics and electron physics, vol. 7. N. Y., Academic, 1955. pp. 239-98.

4) Laegried, N. and G. K. Wehner. "Sputtering yields of metals for Ar^+ and Ne^+ ions with energies from 50 to 600 ev." J. Appl. Phys. 32: 365-69 (1961).

5) Farnsworth, H. E. et al. "Applications of the ion bombardment cleaning method to titanium, germanium, silicon, and nickel as determined by low-energy electron diffraction." J. Appl. Phys. 29: 1150-61 (1958).

6) Handler, P. and W. M. Portnoy. "Electronic surface states and the cleaned germanium surface." Phys. Rev. 116: 516-26 (1959).

7) Hagstrum, H. D. and C. D'Amico. "Production and demonstration of atomically clean metal surfaces." J. Appl. Phys. 31: 715-23 (1960).

8) U. S. Air Technical Intelligence Center. Translation F-TS-9991/V. Tables of electron physics, ion physics and electron microscopy, by M. von Ardenne (1956). Vol. 1, pt. 2, p. 539 (AD 254,521).

9) Langmuir, I. "The effect of space charge and residual gases on thermionic currents in high vacuum." Phys. Rev. 2: 450-86 (1913).

10) Child, C. W. "Discharge from hot lime." Phys Rev. 32: 492-511 (1911).

11) Dushman, S. Scientific foundations of vacuum technique. N. Y., Wiley, 1949.

12) U. S. Air Technical Intelligence Center. Translation F-TS-9991/V. Tables of electron physics, ion physics and electron microscopy, by M. von Ardenne (1956). Vol. 1, pt. 1, p. 79 (AD 254,520).

13) Slater, J. C. and N. H. Frank. Electromagnetism. N. Y., McGraw-Hill, 1947. p. 19.

14) Zworykin, V. K., et al. Electron optics and the electron microscope. N. Y., Wiley, 1945. p. 445.

15) Pierce, J. R. Theory and design of electron beams. 2nd ed. Princeton, N. J., Van Nostrand, 1954. p. 75.

16) U. S. Air Technical Intelligence Center. Translation F-TS-9991/V. Tables of electron physics, ion physics and electron microscopy, by M. von Ardenne (1956). Vol. 1, pt. 2, p. 544 (AD 254,521).

17) Pierce, J. R., op. cit.

18) Kohl, W. H. Materials and techniques for electron tubes. N. Y., Reinhold, 1960.

19) Brown, S. C. Basic data of plasma physics. N. Y., Wiley, 1959.

20) Engel, A. von. "Ionization in gases by electrons in electric fields." In: Handbuch der Physic, vol. 21. Berlin, Springer, 1956. pp. 504-73.

21) Kruithof, A. A. and F. M. Penning. "Determination of the Townsend ionization coefficient for mixtures of neon and argon." Physica 4: 430-49 (1937).

22) Bowden, F. P. and D. Tabor, op. cit.

23) General Mills, Inc. Electronics Group. Report 2255. Investigation of surface phenomena with electron mirror microscopy, by R. C. Menard, A. A. Anderson and W. W. Roepke. (Contract AF 33(616)-6178). Final Report (April 1962) (ARL-62-333).

24) Whitehead, J. R. "Surface deformation and friction of metals at light loads." Proc. Roy. Soc. (London) A201: 109-24 (1950).

25) Page, L. and N. I. Adams. Principles of electricity; an intermediate text in electricity and magnetism. 2nd ed. N. Y., Van Nostrand, 1949.

26) Adam, N. K. The physics and chemistry of surfaces. 2nd ed. Oxford, Clarendon Press, 1938.

27) Patai, I. F. and M. A. Pomerantz. "Contact potential differences." J. Franklin Inst. 252: 239-60 (1951).

28) Kelvin, L. "Contact electricity of metals." Phil. Mag. 46: 82-120 (1898).

29) Zisman, W. A. "A new method of measuring contact potential differences in metals." Rev. Sci. Inst. 3: 368-70 (1932).

30) U. S. Naval Research Laboratory. Report No. 5096. Improvements in the vibrating condenser method of measuring contact potential differences, by K. Bewig (February 1958).

31) Rose, B. A. "Measurements on contact potential difference between different faces of copper single crystals." Phys. Rev. 44: 585-88 (1933).

32) Farnsworth, H. E. and R. P. Winch. "Photoelectric work functions of (100) and (111) faces of silver single crystals and their contact potential difference." Phys. Rev. 58: 812-19 (1940).

33) Hackerman, N. and E. H. Lee. "The effect of gases on the contact potentials of evaporated metal films." J. Phys. Chem. 59: 900-6 (1955).

34) Zisman, W. A. and H. G. Yamins. "Experiments on the contact potential of zinc crystals." Physics 4: 7-9 (1933).

35) Curtis, H. L. and A. H. Scott. "Edge correction in the determination of dielectric constant." Am. Soc. Testing Mater. Proc. 36, 2: 815-29 (1936).

36) Bewig, K. W. and W. A. Zisman. "Low energy reference electrodes for investigating adsorption by contact potential measurements." In: American Chemical Society. Division of Colloid and Surface Chemistry. Solid surfaces and the gas-solid interface. Advances in chemistry series no. 33. Washington, D. C. American Chemical Society, 1961. pp. 100-13.

37) National Research Council. International critical tables of numerical data, physics, chemistry and technology. Vol. 6. N. Y., McGraw-Hill, 1929. p. 57.